Inorg. Chem. **2004**, *43*, 5505–5521

Large Spin Differences in Structurally Related Fe_6 Molecular Clusters and Their Magnetostructural Explanation

Cristina Cañada-Vilalta,[†] Ted A. O'Brien,[†,§] Euan K. Brechin,[†] Maren Pink,[†] Ernest R. Davidson,[†,||] and George Christou*[,†,‡]

Department of Chemistry and the Molecular Structure Center, Indiana University, Bloomington, Indiana 47405-7102, and Department of Chemistry, University of Florida, Gainesville, Florida 32611-7200

Received May 5, 2004

The syntheses, crystal structures, and magnetic characterizations of three new hexanuclear iron(III) compounds are reported. Known $[Fe_6O_2(OH)_2(O_2CBu^t)_{10}(hep)_2]$ (**1**) is converted to new $[Fe_6O_2(OH)(O_2CBu^t)_9(hep)_4]$ (**3**) when treated with an excess of 2-(2-hydroxyethyl)-pyridine (hepH). Similarly, the new compound $[Fe_6O_2(OH)_2(O_2CPh)_{10}(hep)_2]$ (**2**), obtained from the reaction of $[Fe_3O(O_2CPh)_6(H_2O)_3]$ with hepH, is converted to $[Fe_6O_2(OH)(O_2CPh)_9(hep)_4]$ (**4**) when treated with an excess of hepH. This can be reversed by recrystallization from MeCN. The cores of the four Fe_6 complexes all comprise two triangular $[Fe_3(\mu_3\text{-}O)(O_2CR)_3(hep)]^{+3}$ units connected at two of their apices by two sets of bridging ligands. However, **1** and **2** differ slightly from **3** and **4** in the precise way the two Fe_3 units are linked together. In **1** and **2**, the two sets of bridging ligands are identical, consisting of one μ-hydroxo and two μ-carboxylate groups bridging each Fe_2 pair, i.e., a $(\mu\text{-}OH^-)(\mu\text{-}O_2CR^-)_2$ set. In contrast, **3** and **4** have two different sets of bridging ligands, a $(\mu\text{-}OH^-)(\mu\text{-}O_2CR^-)_2$ set as in **1** and **2**, and a $(\mu\text{-}OR^-)_2(\mu\text{-}O_2CR^-)$ set, where RO^- refers to the alkoxide arm of the hep^- chelate. Variable-field and -temperature dc magnetization measurements establish that **1** and **2** have $S = 5$ ground states and significant and positive zero-field splitting parameters (D), whereas **3** and **4** have $S = 0$ ground states. This dramatic difference of 10 unpaired electrons in the ground state S values for near-isomeric compounds demonstrates an acute sensitivity of the magnetic properties to small structural changes. The factors leading to this have been quantitatively analyzed. The semiempirical method ZILSH, based on unrestricted molecular orbital calculations, was used to obtain initial estimates of the Fe_2 pairwise exchange interaction constants (J). These calculated values were then improved by fitting the experimental susceptibility versus T data, using a genetic algorithm approach. The final J values were then employed to rationalize the observed magnetic properties as a function of the core topologies and the presence of spin frustration effects. The large difference in ground state spin value was identified as resulting from a single structural difference between the two types of complexes, the different relative dispositions (*cis* vs *trans*) of two frustrated exchange pathways. In addition, use of the structural information and corresponding J values allowed a magnetostructural correlation to be established between the J values and both the Fe–O bond distances and the Fe–O–Fe angles at the bridging ligands.

Introduction

The last two decades have witnessed an explosive growth in the interest in polynuclear iron(III) compounds with primarily oxygen-based ligation. This has been mainly due to their relevance to two fields, bioinorganic chemistry and molecular magnetism. Iron−oxo centers are found in several non-heme metalloproteins. Hemerythrin, ribonucleotide reductase, and methane monooxygenase are examples of enzymes with di-iron metallosites,[1] whereas the protein ferritin, responsible for iron storage, can accommodate up to ∼4500 iron ions in an iron/oxide/hydroxide core.[2] In the magnetism area, high spin iron(III) ions have a relatively large number of unpaired electrons (d^5, $S = {}^5/_2$) that normally

* To whom correspondence should be addressed. E-mail: christou@chem.ufl.edu.
† Indiana University.
‡ University of Florida.
§ Present address: Department of Chemistry, Indiana University−Purdue University Indianapolis, Indianapolis, IN 46202-3274.
|| Present address: Department of Chemistry, University of Washington, Seattle, WA 98195-1700.

10.1021/ic049413h CCC: $27.50
Published on Web 08/12/2004

undergo strong, antiferromagnetic exchange interactions within multinuclear iron−oxo clusters. With high enough Fe_x nuclearities and appropriate topologies, these compounds can sometimes possess large ground state spin (S) values, and can even occasionally function as single-molecule magnets (SMMs).[3] SMMs are molecules that display slow magnetization relaxation rates and which, below a certain ("blocking") temperature (T_B), can function as single-domain magnetic particles of nanoscale dimensions.[4] In order to be a SMM, a molecule has to fulfill two conditions: It must possess both a ground state with a large spin S, and a significant anisotropy of the easy-axis (Ising) type, as reflected in a large and negative zero-field splitting parameter, D. Although the interactions between Fe^{III} centers are normally antiferromagnetic, certain Fe_x topologies result in large spin ground states because of the occurrence of spin frustration effects. Spin frustration is defined here in its general sense as the occurrence of competing exchange interactions of comparable magnitude that prevent (frustrate) the preferred spin alignments.[5] For example, in certain topologies the spins of two antiferromagnetically coupled metal ions (or other spin carriers) may be forced into a parallel alignment by other, stronger interactions; thus, the intrinsic preference of the spins to align antiparallel is frustrated. An appropriate quantity and distribution of frustrated exchange pathways in some Fe_x topologies can lead to a significantly large value of the total molecular spin, even when all the pairwise Fe_2 exchange interactions are antiferromagnetic.

In this paper, we describe the syntheses, structures, and properties of two Fe_6 complexes with $S = 5$ ground states, $[Fe_6O_2(OH)_2(O_2CR)_{10}(hep)_2]$ (R = Bu^t (**1**), Ph(**2**)), where hep^- is the anion of 2-(2-hydroxyethyl)pyridine). A different crystal form of **1** has been previously reported,[6] whereas its structural analogue **2** is new. Reaction of **1** and **2** with an excess of hepH affords two new compounds $[Fe_6O_2(OH)(O_2CR)_9(hep)_4]$ (R = Bu^t (**3**), Ph (**4**)), with a new type of structure, although similar to that of **1** and **2**. The transformation, which involves the replacement of only two bridging ligands, dramatically changes the ground state spin from $S = 5$ to $S = 0$. We describe the quantitative rationalization of this difference using the results of semiempirical molecular orbital calculations using the recently formulated ZILSH method.[7] These provided initial estimates of all the Fe_2 exchange constants (J), which were then refined by fitting their values to reproduce the experimental variable-temperature magnetic susceptibility of the complexes. The final J values not only correctly predict the observed $S = 0$ vs $S = 5$ spin ground states, but quantitatively rationalize how they come about. Finally, we also describe a magnetostructural correlation between these J values and both the average Fe−O distances and the Fe−O−Fe angles through the shortest Fe−O−Fe pathway of interaction. This should prove extremely useful in the future for predicting and/or rationalizing the magnetic properties of new multinuclear Fe(III) complexes, and how those properties might be affected by relatively small structural changes.

Experimental Section

Syntheses. All manipulations were performed under aerobic conditions using chemicals as received, unless otherwise stated. $[Fe_6O_2(OH)_2(O_2CBu^t)_{10}(hep)_2]$ (**1**) [6] and $[Fe_{11}O_6(OH)_6(O_2CPh)_{15}]$[8] were prepared as described in the literature; hepH is 2-(2-hydroxyethyl)pyridine.

$[Fe_3O(O_2CPh)_6(H_2O)_3]$. A stirred solution of $FeCl_2 \cdot 4H_2O$ (3.00 g, 15.1 mmol) and sodium benzoate (6.52 g, 45.3 mmol) in water (60 mL) was treated with a solution of benzoic acid (11.1 g, 90.5 mmol) in acetonitrile (60 mL). The mixture was boiled for 30 min and then cooled to room temperature. The resulting precipitate was collected by filtration and washed with a copious amount of water and a little acetonitrile, in which the compound is partially soluble. The material was vacuum-dried; yield, 69%. Anal. Calcd (Found) for $C_{42}H_{36}Fe_3O_{16}$: C, 52.31 (52.47); H, 3.76 (3.56)%. Selected IR data (KBr, cm^{-1}): 1600(vs); 1560(vs); 1492(s); 1420(s); 1392(vs); 1295(m); 1176(m); 1147(w); 1071(w); 1025(m); 1002(w); 940(w); 840(w); 818(w); 721(s); 673(s); 593(m); 464(s).

$[Fe_3O(O_2CPh)_6(H_2O)_3](NO_3)$. A stirred solution of $Fe(NO_3) \cdot 9H_2O$ (1.6 g, 5.8 mmol) in water (20 mL) was treated with a solution of sodium benzoate (3.5 g, 24 mmol) in water (30 mL). A light orange precipitate was obtained immediately. The solid was collected by filtration, washed with copious amounts of water, and dried under vacuum; yield, 82%. Selected IR data (KBr, cm^{-1}): 3408(br); 3062(m); 1700(m); 1601(s); 1564(s); 1410(vs); 1177(m); 1070(m); 1025(m); 1002(w); 940(w); 841(w); 819(w); 717(s); 686(m); 675(m); 631(m); 484(s).

$[Fe_6O_2(OH)_2(O_2CPh)_{10}(hep)_2]$ (2). Method A. A solution of $[Fe_3O(O_2CPh)_6(H_2O)_3]$ (0.25 g, 0.26 mmol) in acetonitrile (20 mL) was boiled gently for 5 min, and then a solution of hepH (94 mg, 0.76 mmol) in acetonitrile was slowly added. After 5 min more, the solution was filtered hot, and the filtrate was allowed to cool slowly. Orange crystals formed after a few hours, and these were collected by filtration, washed with a little acetonitrile, and dried under vacuum; yield, 49%. Dried solid analyzed as solvent-free.

(1) (a) Kurtz, D. M., Jr. *Chem. Rev.* **1990**, *90*, 585. (b) Lippard, S. J. *Angew. Chem., Int. Ed. Engl.* **1988**, *27*, 344. (c) Toftlund, H.; Murray, K. S.; Zwack, P. R.; Taylor, L. F.; Anderson, O. P. *J. Chem. Soc., Chem. Commun.* **1986**, 191.

(2) (a) Theil, E. C. *Annu. Rev. Biochem.* **1987**, *57*, 289 and references therein. (b) Xu, B.; Chasteen, N. D. *J. Biol. Chem.* **1991**, *266*, 19965.

(3) (a) Christou, G.; Gatteschi, D.; Hendrickson, D. N.; Sessoli, R. *MRS Bull.* **2000**, *25*, 66 and references therein. (b) Hendrickson, D. N.; Christou, G.; Ishimoto, H.; Yoo, J.; Brechin, E. K.; Yamaguchi, A.; Rumberger, E. M.; Aubin, S. M.; Sun, Z.; Aromí, G. *Polyhedron* **2001**, *20*, 1479. (c) Gatteschi, D.; Sessoli, R.; Cornia, A. *Chem. Commun.* **2000**, *9*, 725, and references therein.

(4) (a) Soler, M.; Rumberger, E.; Folting, K.; Hendrickson, D. N.; Christou, G. *Polyhedron* **2001**, *20*, 1365. (b) Soler, M.; Chandra, S. K.; Ruiz, D.; Huffman, J. C.; Hendrickson, D. N.; Christou, G. *Polyhedron* **2001**, *20*, 1279. (c) Aubin, S. M.; Sun, Z.; Eppley, H. J.; Rumberger, E. M.; Guzei, I. A.; Folting, K.; Gantzel, P.; Rheingold, A. L.; Christou, G.; Hendrickson, D. N. *Polyhedron* **2001**, *20*, 1139. (d) Sañudo, E. C.; Grillo, V. A.; Yoo, J.; Huffman, J. C.; Bollinger, J. C.; Hendrickson, D. N.; Christou, G. *Polyhedron* **2001**, *20*, 1269.

(5) (a) McCusker, J. K.; Vincent, J. B.; Schmitt, E. A.; Mino, M. L.; Shin, K.; Coggin, D. K.; Hagen, P. M.; Huffman, J. C.; Christou, G.; Hendrickson, D. N. *J. Am. Chem. Soc.* **1991**, *113*, 3012−3021. (b) Libby, E.; McCusker, J. K.; Schmitt, E. A.; Folting, K.; Hendrickson, D. N.; Christou, G. *Inorg. Chem.* **1991**, *31*, 3486. (c) Khan, O. *Chem. Phys. Lett.* **1997**, *265*, 109.

(6) Cañada-Vilalta, C.; Rumberger, E.; Brechin, E. K.; Wernsdorfer, W.; Folting, K.; Davidson, E. R.; Hendrickson, D. N.; Christou, G. *J. Chem. Soc., Dalton Trans.* **2002**, *21*, 4005.

(7) O'Brien, T. A.; Davidson, E. R. *Int. J. Quantum Chem.* **2003**, *92*, 294.

(8) Gorun, S. M.; Papaefthymiou, G. C.; Frankel, R. B.; Lippard, S. J. *J. Am. Chem. Soc.* **1987**, *109* (11), 3337.

Anal. Calcd (Found) for $C_{84}H_{68}Fe_6N_2O_{26}$: C, 54.34 (53.81); H, 3.69 (3.55); N, 1.51 (1.58)%. Selected IR data (KBr, cm^{-1}): 3440(br); 2923(vw); 2888(vw); 2854(w);1598(s); 1554(s); 1527(m); 1492(m); 1405(vs); 1314(w); 1251(w); 1177(m); 1157(w); 1113(w); 1082(m); 1068(m); 1026(m); 718(s); 689(m); 673(m); 661(m); 595(m); 538(m); 474(s), 430(m).

Method B. A solution of $[Fe_3O(O_2CPh)_6(H_2O)_3](NO_3)$ (0.20 g, 0.19 mmol) in hot acetonitrile (15 mL) was treated with hepH (72 mg, 0.57 mmol) in acetonitrile (3 mL). The resulting mixture was boiled gently for 5 min, filtered, and then allowed to cool to room temperature. Microcrystals formed within minutes, and these were collected by filtration and washed with acetonitrile; yield, 31%. The product was identified by IR comparison with material from method A.

Method C. Compound **4** (0.1 g, 0.05 mmol) was stirred in hot acetonitrile (15 mL) for several hours. The very pale orange solution was then filtered hot to remove undissolved starting material, and the filtrate was allowed to cool slowly to room temperature. Crystals of **2** formed over several hours, and these were collected by filtration and washed with acetonitrile. The product was identified by IR comparison with material from method A.

$[Fe_6O_2(OH)(O_2CBu^t)_9(hep)_4]$ (3). A suspension of compound **1** (0.20 g, 0.12 mmol) in hot acetonitrile (15 mL) was treated with an excess of hepH (0.5 g, 4.1 mmol). The mixture was stirred overnight at 50 °C, filtered to remove some undissolved starting material, and allowed to stand undisturbed in closed vials at room temperature. Brown crystals suitable for X-ray crystallography formed over a week in 20% yield. Selected IR data (KBr, cm^{-1}): 3414(w,br), 2957(s), 2926(m), 2867(m), 1559(vs), 1483(vs), 1422(vs), 1376(s), 1360(s), 1314(w), 1229(s), 1156(w), 1111(m), 1082(m), 1048(m), 1022(m), 972(vw), 937(vw), 895(w), 787(m), 762(w), 672(m), 604(s), 543(m), 432(s).

$[Fe_6O_2(OH)(O_2CPh)_9(hep)_4]$ (4). Method A. A solution of $[Fe_{11}O_6(OH)_6(O_2CPh)_{15}]$ (0.16 g, 0.065 mmol) in acetonitrile was boiled gently for 10 min and then treated with a solution of hepH (87 mg, 0.71 mmol) in MeCN (3 mL). The solution was boiled for an additional 5 min, and then filtered hot and left undisturbed overnight at room temperature. The resulting crystals were collected by filtration, washed with a little acetonitrile, and dried under vacuum; yield, 47%. Dried solid analyzed as solvent-free. Anal. Calcd (Found) for $C_{91}H_{78}Fe_6N_4O_{25}$: C, 55.69 (55.24); H, 3.98 (3.96); N, 2.86 (2.50) %. Selected IR data (KBr, cm^{-1}): 3654(vw); 3398(br); 3064(w); 2932(w); 2849(w); 1592(s); 1548(s); 1492(m); 1400(vs); 1313(w); 1254(w); 1175(m); 1156(w); 1111(w); 1069(m); 1049(m); 1025(m); 839(w); 765(w); 717(s); 689(m); 673(m); 593(m); 542(m); 470(s).

Method B. Compound **2** (0.20 g, 0.11 mmol) was slurried in acetonitrile (15 mL) and treated with an excess of hepH (0.5 g, 4 mmol). The mixture was stirred and heated for several hours, after which it was filtered hot and the filtrate left undisturbed for several days at room temperature. The resulting crystals were collected by filtration, washed with a little acetonitrile, and dried under vacuum. The product was identified by IR comparison with material from method A.

X-ray Crystallography. X-ray crystallography data were collected on a SMART 6000 (Bruker) diffractometer. Suitable crystals were attached to the tip of a glass capillary and transferred to the goniostat, where they were cooled for characterization and data collection using Mo Kα radiation (graphite monochromator). The structures were solved using SIR-92[9] and SHELXL-97,[10] and refined by full-matrix least-squares cycles. Data collection parameters and structure solution and refinement details are listed in Table 1.

Table 1. Crystallographic Data for $[Fe_6O_2(OH)_2(O_2CBu^t)_{10}(hep)_2]$ (**1**), $[Fe_6O_2(OH)_2(O_2CPh)_{10}(hep)_2]$ (**2**), $[Fe_6O_2(OH)(O_2CBu^t)_9(hep)_4]$ (**3**), and $[Fe_6O_2(OH)(O_2CPh)_9(hep)_4]\cdot 3MeCN$ (**4**·3MeCN)

	1	**2**	**3**	**4**·3 MeCN
formula[a]	$C_{64}H_{108}Fe_6N_2O_{26}$	$C_{84}H_{68}Fe_6N_2O_{26}$	$C_{73}H_{114}Fe_6N_4O_{25}$	$C_{96.18}H_{86.34}Fe_6N_7O_{25}$
fw, g/mol	1656.64	1856.50	1782.80	2075.26
space group	$P2_1/n$	$P2_1/c$	$C2/c$	$P\bar{1}$
a, Å	11.8387(9)	12.5022(5)	27.483(1)	12.9519(6)
b, Å	22.275(2)	25.052(1)	13.9180(6)	14.2296(7)
c, Å	14.899(1)	13.6514(6)	46.913(2)	26.411(1)
α, deg	90	90	90	89.1090(1)
β, deg	94.898(2)	113.541(1)	93.934(1)	83.2400(1)
γ, deg	90	90	90	83.0730(1)
V, Å^3	3914.5(1)	3919.8(3)	17902(1)	4798.4(4)
Z	2	2	8	2
ρ calcd, g/cm^3	1.405	1.573	1.323	1.436
T, °C	−163	−168	−158	−168
radiation,[b] Å	0.71073	0.71073	0.71073	0.71073
μ, cm^{-1}	1.156	11.639	10.153	9.61
R1 (wR2),[c] %	5.3 (14.3)	4.6 (12.1)	4.74 (11.1)	5.59 (15.8)

[a] Including solvate molecules. [b] Graphite monochromator. [c] $R1 = 100\sum||F_o| - |F_c||/\sum|F_o|$. $wR2 = 100[\sum[w(F_o^2 - F_c^2)^2]/\sum[w(F_o^2)^2]]^{1/2}$.

The new crystalline form of $[Fe_6O_2(OH)_2(O_2CBu^t)_{10}(hep)_2]$ (**1**) with no solvent of crystallization[6] was obtained by slow evaporation of a saturated solution in dichloromethane. The compound crystallizes in the monoclinic space group $P2_1/n$. The structure is centrosymmetric with the asymmetric unit containing half of the Fe_6 complex. A direct-methods solution was calculated that located all non-hydrogen atoms from the electron density map, and these were refined with anisotropic displacement parameters. All hydrogen atoms were placed in calculated, ideal positions and refined as riding atoms with isotropic displacement parameters set to be a multiple of that of the parent atom. The final full-matrix least-squares refinement on F^2 converged to $R = 5.34\%$ ($I > 2\sigma(I)$) and $wR2 = 14.29\%$ (all data). The remaining electron density is located around the Fe atoms. One of the Bu^t groups is disordered over two positions, which refined to 54% and 46% occupancies.

$[Fe_6O_2(OH)_2(O_2CPh)_{10}(hep)_2]$ (**2**) crystallizes in the monoclinic space group $P2_1/c$. The structure is again centrosymmetric with the asymmetric unit containing half of the Fe_6 molecule and no solvent molecules. All non-hydrogen atoms were located by a combination of direct methods and difference Fourier map calculation, and refined with anisotropic displacement parameters. Hydrogen atoms were placed in ideal positions, as for **1**, and refined with isotropic displacement parameters. The only exception was H2, involved in a hydrogen bond with O11 of a benzoate group, which was found in a difference map and refined for all parameters. R1 and wR2 for the final full-matrix least-squares refinement on F^2 were 4.6% ($I > 2\sigma(I)$) and 12.1% (all data), respectively. The final difference Fourier map was essentially featureless, with the remaining electron density located in the vicinity of the metal atoms.

$[Fe_6O_2(OH)(O_2CBu^t)_9(hep)_4]$ (**3**) crystallizes in the monoclinic space group $C2/c$. A direct methods solution was obtained that provided most of the non-hydrogen atoms, and the remaining non-hydrogen atoms were located by full-matrix least-squares and difference Fourier map cycles. Disorder was refined in two Me and one hep^- groups. All non-hydrogen atoms were refined with anisotropic displacement parameters. The hydrogen atoms were

(9) Altomare, A.; Cascarno, G.; Giacovazzo, C.; Gualardi, A. *J. Appl. Crystallogr.* **1993**, *26*, 343.

(10) *SHELXTL-Plus* V5.10; Bruker Analytical X-ray Systems: Madison, WI.

again placed in ideal positions and refined with isotropic displacement parameters, except for H3, which is involved in a strong hydrogen bond with O25 and was refined for all parameters. The final full-matrix least-squares refinement on F^2 converged to R1 = 4.74% ($I > 2\sigma(I)$) and wR2 = 11.1% (all data). Remaining electron density and large displacement parameters for several methyl groups and the second nonchelating hep$^-$ group suggest some further, unresolved disorder. Attempts to refine such disorders did not yield any improvement in the final residuals and thermal parameters.

$[Fe_6O_2(OH)(O_2CPh)_9(hep)_4]\cdot 3MeCN$ (**4**·3MeCN) crystallizes in the triclinic space group $P\bar{1}$. The asymmetric unit contains one Fe_6 molecule and three molecules of solvent. A structure solution by direct methods located most of the non-hydrogen atoms; the remaining non-hydrogen atoms were located by full-matrix least-squares and difference Fourier map cycles. Non-hydrogen atoms were refined using anisotropic displacement parameters, whereas all hydrogen atoms were placed in ideal positions and refined with isotropic displacement parameters riding on those of the parent atom. The crystal exhibits two kinds of disorder. First, disordered acetonitrile molecules were found in a solvent channel; second, a nonchelating hep$^-$ molecule is disordered with a hydroxide group (84% and 16%, respectively), hydrogen-bonded to an acetonitrile molecule. The figures and calculations described in this paper refer to the majority species, i.e., when the bridging group is hep$^-$. The final full-matrix least-squares refinement on F^2 converged to values of R1 and wR2 of 5.59% ($I > 2\sigma(I)$) and 15.8% (all data), respectively. The final difference Fourier map shows remaining electron density near the disordered hep$^-$ molecule, indicating that additional solvent molecules (most likely water) may be involved in the disorder.

Computational Methods. The exchange interactions in **1**−**4** were calculated using the recently developed semiempirical ZILSH method.[7,11] The method uses molecular orbital (MO) calculations with the intermediate neglect of differential overlap Hamiltonian parametrized for optical spectroscopy (INDO/S) of Zerner[12,13] to obtain energies for various alignments of the spins of the metal ions in a polynuclear transition metal complex. A semiempirical application[7,11] of Davidson's local spin operator[14,15] was used to obtain spin couplings between metal ions, $\langle \hat{S}_A \cdot \hat{S}_B \rangle$, from the semiempirical wave functions. Together with the energies, these quantities were used to obtain estimates of the exchange constants J_{AB} that appear in the Heisenberg spin Hamiltonian (HSH) of eq 1

$$\hat{H} = \hat{H}_0 - 2\sum_{A<B} J_{AB}\hat{S}_A \cdot \hat{S}_B \tag{1}$$

where $\hat{H}_0$ contains all spin-independent terms. The HSH gives the energies of the spin states of the complex as in eq 2

$$E_i = E_0 - 2\sum_{A<B} J_{AB}\langle \hat{S}_A \cdot \hat{S}_B \rangle^i \tag{2}$$

where E_0 contains spin-independent contributions to the energy, such as electron−nuclear attractions. Given the energies and spin couplings of a number of spin components equal to the number of parameters J_{AB} and E_0, eq 2 can be solved simultaneously for the parameter values.

The large size and complex electronic structure of polynuclear transition metal complexes makes the application of a basis of spin states prohibitive. Instead of spin state wave functions that are linear combinations of many determinants, ZILSH uses single determinant wave functions, composed of a single set of MOs. The MOs are optimized with the unrestricted Hartree−Fock self-consistent field (UHF-SCF) formalism.[16] The local spin operator allows expectation values $\langle \hat{S}_A.\hat{S}_B \rangle^{UHF}$ to be computed for the MO wave functions. Under certain conditions (discussed below),[7] the energies of the MO wave functions are given by eq 2 with $\langle \hat{S}_A.\hat{S}_B \rangle^{UHF}$ and the same exchange constants that describe the true spin states of the system. This means that the exchange constants obtained are of comparable accuracy regardless of the total spin of the wave function (see ref 7 for discussion). For complexes of modest size, the energies and compositions of the spin states can be examined by substituting the exchange constants into the HSH and diagonalizing in a basis of components $|S_1 \cdot M_1\rangle|S_2 \cdot M_2\rangle ... |S_N \cdot M_N\rangle$, where S_A and M_A are, respectively, the spin and z-component of spin for metal center A (e.g., $S_A = {}^5/_2$ for high spin Fe^{3+} ions).

Exchange constants found with ZILSH contain errors due to using approximate UHF wave functions rather than spin states, and errors in energies inherent in the semiempirical parametrization of the INDO/S method. Considering the former, it has been demonstrated that if the single determinant wave functions are high spin eigenfunctions of the local spin operators for the metal center spins, then the correct exchange constants are obtained regardless of the total spin of the wave function. In practice, UHF wave functions rarely meet this requirement. The size of this error can be judged in two ways. First, the expectation values of local spin for the metal centers can be compared to what would be obtained for high spin metal centers. In the case of Fe^{3+} ions, for example, the local spin quantum number is $S_A = {}^5/_2$, so the expectation value $\langle \hat{S}^2_A \rangle = S_A(S_A + 1)$ would be 8.75. Second, the expectation value of the total spin operator, $\langle \hat{S}^2 \rangle^{UHF}$, can be compared to the value expected for single determinant wave functions in which the local spin operators for the metals have high-spin eigenvalues. This expectation value, $\langle \hat{S}^2 \rangle^{LS}$, is given by eq 3.

$$\langle S^2 \rangle^{LS} = M^2 + M^{max} \tag{3}$$

Both of these measures are used to assess the accuracy of the exchange constants obtained for complexes **1**, **2**, **3**, and **4**.

Even when the error due to using approximate wave functions is small, the error inherent in the INDO/S parameters remains. Consequently, a genetic algorithm method for refining the exchange constants to better reflect experimental data was implemented.[7] This method uses the Van Vleck equation[17] to relate the product of the magnetic susceptibility and temperature to the exchange constants, as described elsewhere.[7] The exchange constants, electronic g factor, and temperature-independent paramagnetism (TIP) are all adjusted simultaneously to minimize the differences between experimental and calculated values of $\chi_m T$ for temperatures above 25 K. Lower temperatures are excluded because other factors such as zero-field splitting of low-lying states (which are not obtained from the calculations) and intermolecular interactions become operative below 25 K. Exchange constants calculated with ZILSH are used

(11) O'Brien, T. A.; Cañada-Vilalta, C.; Christou, G.; Davidson, E. R. *J. Phys. Chem. A*, in press.
(12) Zerner, M. C.; Loew, G. H.; Kirchner, R. F.; Mueller-Westerhoff, U. T. *J. Am. Chem. Soc.* **1980**, *102*, 589−599.
(13) Zerner, M. C. *Semiempirical Molecular Orbital Methods*; Lipkowitz, K. B., Boyd, D. B., Eds.; VCH: New York, 1991; Vol. 2, pp 313−363.
(14) Clark, A. E.; Davidson, E. R. *J. Chem. Phys.* **2001**, *115*, 7382−7392.
(15) Davidson, E. R.; Clark, A. E. *Mol. Phys.* **2002**, *100*, 373−383.
(16) Szabo, A.; Ostlund, N. S. *Modern Quantum Chemistry: Introduction to Advanced Electronic Structure Theory*; McGraw-Hill: New York, 1989.
(17) Van Vleck, J. H. *The Theory of Electric and Magnetic Susceptibilities*; Oxford Press: London, 1932.

Scheme 1

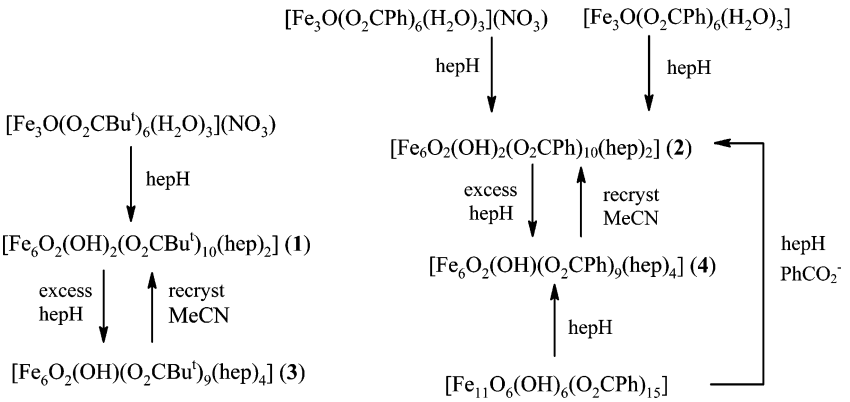

as starting guesses, and the *g* factor is allowed to vary between 1.90 and 2.00. Similarly, the TIP is allowed to vary between 900 $\times 10^{-6}$ and 1200 $\times 10^{-6}$ cm^3 mol^{-1}. The final, refined exchange constants are substituted into the HSH, which is diagonalized to give the spin state energies and wave functions. The latter are linear combinations of components defined by different orientations of the metal center spins (eq 4)

$$|SM\rangle = \sum_i C_i^M |S_1 M_1^i\rangle |S_2 M_2^i\rangle \cdots |S_N M_N^i\rangle \qquad (4)$$

where S is the total spin, M is the z-component of total spin, and C_i^M are expansion coefficients. The local z-components are restricted according to $M = M_1^i + M_2^i + ... + M_N^i$. In describing wave functions for complexes **1**, **2**, **3**, and **4**, we use the more compact notation $|M_1^i M_2^i ... M_N^i\rangle$ to represent a component.

Two other quantities are important for analyzing spin alignments in the spin states. One is the expectation value of the z-components of spin of the metal centers, $\langle M_A \rangle$, which are a direct indication of spin alignments. The other is the expectation value $\langle \hat{S}_A \cdot \hat{S}_B \rangle$ that appears in the HSH (not to be confused with the similar quantity computed for a UHF component, discussed above), which is useful for examining spin alignments in singlet states, where all $\langle M_A \rangle$ are zero. Also, $\langle \hat{S}_A \cdot \hat{S}_B \rangle$ is useful for analyzing spin frustration effects because it represents the actual alignment of the spins of metal centers A and B in the spin state (whereas J indicates the preferred alignment), and is positive and negative for parallel and antiparallel alignment, respectively. Thus, if $\langle \hat{S}_A \cdot \hat{S}_B \rangle$ and J_{AB} differ in sign, the A−B pathway is frustrated. In a more quantitative sense, the product $-2J_{AB}\langle \hat{S}_A \cdot \hat{S}_B \rangle$ represents the contribution made by the A−B pathway to the total energy of the spin state. If they have different signs (i.e., if the interaction is frustrated), the total energy is increased by the interaction of spins. The product $-2J_{AB}\langle \hat{S}_A \cdot \hat{S}_B \rangle$ was used to identify frustrated pathways in complexes **1**, **2**, **3**, and **4**.

One caveat regarding the method just described is that there are more spin components than parameters for complexes with more than three metals. In the case of the Fe_6 complexes considered here, for example, there are 32 unique ways of reversing spins of the metals, while there are only 16 parameters (J_{AB} and E_0). A question that naturally arises is if the same exchange constants are obtained for different choices of spin components. This has not yet been examined in detail, but it was found by trial and error that very similar values of the parameters were obtained for different choices for the complex $[Fe_6O_2(OH)_2(O_2CCH_3)_{10}(C_{10}H_{13}N_4O)_2]$[18,19,22]. Additionally, it has been demonstrated that if the component wave functions are high spin eigenfunctions of the local spin operators for the metal center spins (a condition approximately met by the wave functions found in this work, vide infra), the exchange constants found from any set of spin components are formally equivalent.[7] See ref 7 for a detailed discussion of this question.

Other Studies. Infrared spectra were recorded in the solid state (KBr pellets) on a Nicolet model 510P FTIR spectrophotometer in the 4000−400 cm^{-1} range. Elemental analyses (C, H, and N) were performed on a Perkin-Elmer 2400 Series II analyzer. Magnetic measurements were performed on a Quantum Design MPMS-XL SQUID magnetometer equipped with a 7 T magnet. Pascal's constants were used to estimate the diamagnetic correction, which was subtracted from the experimental susceptibility to give the molar paramagnetic susceptibility (χ_M).

Results and Discussion

Syntheses. For convenience, the various preparations and transformations described below are summarized in Scheme 1.

We recently reported elsewhere[6] the preparation of $[Fe_6O_2(OH)_2(O_2CBu^t)_{10}(hep)_2]$ (**1**) from the reaction of $[Fe_3O(O_2CBu^t)_6(H_2O)_3](NO_3)$ with 3 equiv of hepH. An analogous procedure was employed here to synthesize $[Fe_6O_2(OH)_2(O_2CPh)_{10}(hep)_2]$ (**2**). Thus, $[Fe_3O(O_2CPh)_6(H_2O)_3](NO_3)$ was dissolved in hot acetonitrile and treated with 3 equiv of hepH to yield red crystals of **2** upon cooling. The reaction is summarized in eq 5; note that both the ligand hepH and the released $PhCO_2^-$ groups can act as proton acceptors to facilitate formation of OH^- and hep^- groups.

$$2[Fe_3O(O_2CPh)_6(H_2O)_3]^+ + 4hepH \rightarrow [Fe_6O_2(OH)_2(O_2CPh)_{10}(hep)_2] + 2hepH_2^+ + 2PhCO_2H + 4H_2O \qquad (5)$$

Similar results were obtained when neutral $[Fe_3O(O_2CPh)_6(H_2O)_3]$ was employed as the starting material. This complex is mixed valent ($Fe^{II}Fe_2^{III}$), but air oxidation proved sufficient to yield the all-Fe^{III} product in high yield (49%). Although there is no easy way to study the mechanism of formation of **1** and **2**, their structures suggest that the hep^- groups have

(18) McCusker, J. K.; Christmas, C. A.; Hagen, P. M.; Chadha, R. K.; Jarvey, D. F.; Hendrickson, D. N. *J. Am. Chem. Soc.* **1991**, *113*, 6114.

(19) Christmas, C. A.; Tsai, H.-L.; Pardi, L.; Kesselman, J. M.; Gantzel, P. K.; Chadha, R. K.; Gatteschi, D.; Jarvey, D. F.; Hendrickson, D. N. *J. Am. Chem. Soc.* **1993**, *115*, 12483.

induced a dimerization of two [$Fe_3(\mu_3$-O)] units with little change to the individual [Fe_3-(μ_3-O)] cores.

When complexes **1** and **2** were treated in acetonitrile with an excess of hepH, the latter was incorporated into one of the two inter-Fe_3 connections between vertices. Two hep^- groups, which employ their alkoxide arms to bridge, replace a μ-carboxylate group and the μ-hydroxide groups, the N atoms of these hep^- ligands remaining uncoordinated. It is interesting that extra hep^- groups are only incorporated into one of the inter-Fe_3 sets of bridging ligands. The conversion is summarized in eq 6.

$$[Fe_6O_2(OH)_2(O_2CR)_{10}(hep)_2] + 2hepH \rightarrow [Fe_6O_2(OH)(O_2CR)_9(hep)_4] + RCO_2H + H_2O \quad (6)$$

In the case of benzoate complex **4**, the crystal structure revealed a disorder at one of the bridging hep^- groups, whose site is still occupied by the μ-OH^- group in 16% of the molecules. This might indicate that the ligand substitution takes place in a sequential fashion, with a carboxylate substituted first, followed by the hydroxide group.

The conversion of **1** and **2** to **3** and **4**, respectively, is reversible. Recrystallization of **3** and **4** from hot acetonitrile gives **1** and **2**, respectively. The conversion is sacrificial since no additional carboxylate was added, and the yields were accordingly not high.

An alternative route was found to **4** involving treatment of [$Fe_{11}O_6(OH)_6(O_2CPh)_{15}$] with 11 equiv of hepH, which gave compound **4** in good yield (47%), as summarized in eq 7.

$$9[Fe_{11}O_6(OH)_6(O_2CPh)_{15}] + 99hepH \rightarrow 15[Fe_6O_2(OH)(O_2CPh)_9(hep)_4] + 9Fe^{3+} + 27hep^- + 6hepH + 63H_2O \quad (7)$$

The reason for the formation of **4** instead of **2** probably lies in the lower availability of benzoate ligand, which is the limiting reagent in this reaction. The Fe_{11} starting material contains ~1.4 benzoate groups per Fe, as opposed to the two per Fe in $[Fe_3O(O_2CPh)_6(H_2O)_3]^{0/+}$. In accord with this, the same reaction but also with 7 equiv of sodium benzoate per Fe_{11} (enough to give a total of two benzoates per Fe) now gave **2** instead of **4**. However, when the reaction was carried out with benzoic acid instead of benzoate, the product was **4**.

Description of Structures. [$Fe_6O_2(OH)_2(O_2CBu^t)_{10}(hep)_2$] (1) and [$Fe_6O_2(OH)_2(O_2C-Ph)_{10}(hep)_2$] (2). Labeled ORTEP plots of [$Fe_6O_2(OH)_2(O_2CPh)_{10}(hep)_2$] (**2**) from two viewpoints are presented in Figure 1; ORTEP plots of [$Fe_6O_2(OH)_2(O_2CBu^t)_{10}(hep)_2$] (**1**) are available elsewhere,[6] and are very similar to those for **2**. Selected bond distances and angles comparing **1** and **2** with **3** and **4** are listed in Table 2; the data for **1** are from this work for the nonsolvated, monoclinic form. Compounds **1** and **2** crystallize in monoclinic space groups and display crystallographic C_i symmetry; the asymmetric units therefore contain only half of an Fe_6 molecule, and there are no solvent molecules in the cell. The structure comprises six Fe atoms in an almost planar

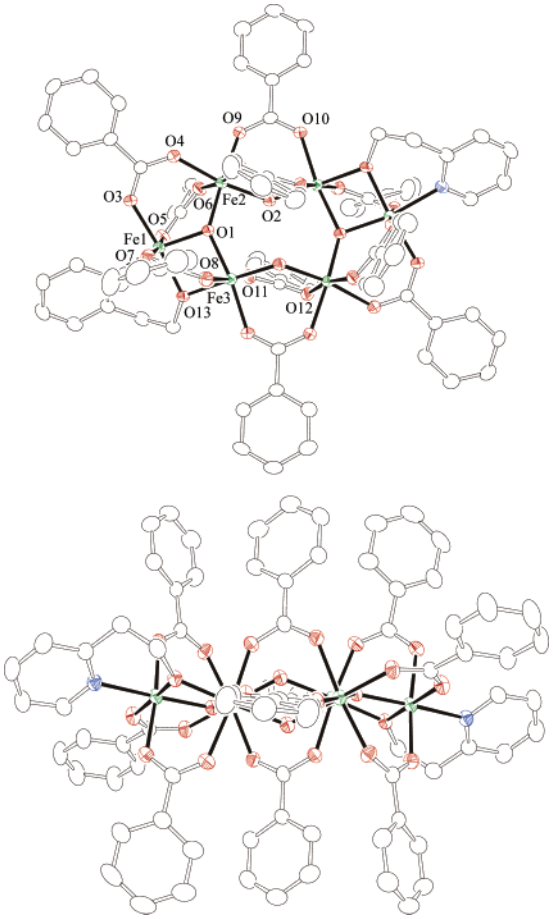

Figure 1. ORTEP representations of [$Fe_6O_2(OH)_2(O_2CPh)_{10}(hep)_2$] (**2**) from viewpoints perpendicular to, and along, the plane formed by the six Fe atoms. Atoms are drawn at the 50% probability level, and hydrogen atoms have been omitted for clarity.

arrangement that can be described as two triangular [$Fe_3(\mu_3$-O)] units joined together at two of their apices. Each linkage comprises one bridging hydroxide and two bridging carboxylate groups, with the Fe−O(H)−Fe angle being 121.6(1)° for **1** and 125.6(2)° for **2**. The μ_3-oxide in each triangular unit is slightly out of the plane formed by the three Fe atoms (Fe1, Fe2, and Fe3) by 0.263 Å in **1** and 0.195 Å in **2**. Each Fe_3 triangle is scalene. In addition to the central μ_3-oxide ion, Fe1 and Fe2 are bridged by two μ-O_2CR^- groups, whereas Fe1 and Fe3 are linked by one μ-O_2CR^- group and a μ-alkoxo group from a hep^- ligand. Note that there are two monatomic bridges between Fe1 and Fe3, and this causes this Fe···Fe distance (2.9−3.0 Å) to be significantly shorter than the other two (3.2−3.3 and 3.5−3.6 Å). All the Fe atoms possess distorted octahedral coordination geometries. The overall structure is slightly distorted by the presence of intramolecular hydrogen bonds between the bridging hydroxo group and one of the oxygen atoms from the distal O_2CR^- group. This is evidenced by the short separation of 2.926(2) Å between O2 and O11 in **2** (2.812(2) Å in **1**).

For convenience in comparing the overall structures of **1** and **2** with **3** and **4**, we will refer to the former as possessing a *trans* topology, referring to the relative disposition of the two short, monatomically bridged Fe_2 pairs; as will be described below, **3** and **4** are then the *cis* isomer of this Fe_6

Table 2. Principal Structural Parameters (Å, deg) for Complexes **1**−**4**

label[a]	**1**[b]	**2**[b]	**3**[c]	**4**[c]
		Fe···Fe		
A	3.253(2)	3.270(7)	3.3080(4), 3.2638(4)	3.285(6), 3.279(6)
B	3.570(2)	3.603(7)	3.5824(4), 3.5627(4)	3.587(6), 3.598(6)
C	2.933(2)	2.918 (7)	2.9185(4), 2.9390(4)	2.943(6), 2.935(7)
D	3.428(2)	3.488(7)	3.4423(4)	3.444(6)
E			3.0753(4)	3.091(6)
		Fe−O		
a	1.900 (2)	1.915(2)	1.901(2), 1.880(1)	1.905(2), 1.897(2)
b	1.884(2)	1.871(2)	1.893(2), 1.882(2)	1.883(2), 1.886(2)
c	1.961(2)	1.967(2)	1.955(2), 1.936(2)	1.964(2), 1.969(2)
d	1.972(2)	1.976(2)	1.980(2), 2.000(2)	1.982(2), 1.993(2)
e	2.001(2)	1.998(2)	1.990(2), 2.033(2)	1.992(2), 1.993(2)
f	1.947(2), 1.979 (2)	1.940(3), 1.981(3)	1.951(2), 1.951(2)	1.933(2), 1.948(2)
g			2.012(2), 2.020(2)	2.031(2), 2.033(2)
h			1.967(2), 1.990(2)	1.983(2), 1.974(2)
		Fe−O−Fe		
α	118.6(1)	119.5(1)	121.38(8), 120.38(8)	120.3(1), 120.2(1)
β	136.4(1)	139.6(1)	137.16(8), 137.90(8)	137.7(1), 137.9(1)
γ	98.9(1)	97.5(1)	98.39(7), 100.74(7)	99.1(1), 98.74(9)
δ	95.2(1)	94.5(1)	93.56(7), 94.65(7)	95.60(9), 94.88(8)
ϵ	121.6(1)	125.6(2)	124.07(9)	125.1(1)
ζ			99.43(7)	99.03(9)
θ			102.02(7)	102.7(1)

[a] Labels refer to those in Figure 2. [b] Crystallographic C_i symmetry. [c] Virtual C_s symmetry; entries are grouped together under this symmetry.

topology (Figure 2). Two other complexes with an overall structure the same as **1** and **2**, and thus also of the *trans* type, have been previously reported, containing acetate as the carboxylate ligand and imidazole-based ligands as the chelating groups: $[Fe_6O_2(OH)_2(O_2CMe)_{10}(C_{10}H_{13}N_4O)_2]$[18] and $[Fe_6O_2(OH)_2(O_2CMe)_{10}(C_7H_{11}N_2O)_2]$.[19]

$[Fe_6O_2(OH)(O_2CBu^t)_9(hep)_4]$(3) and $[Fe_6O_2(OH)(O_2CPh)_9(hep)_4]\cdot 3MeCN$ (4·3MeCN). Compounds **3** and **4** have very similar structures and will therefore be described together; labeled ORTEP plots are presented in Figures 3 and 4. Compound **3** crystallizes without any solvent molecules in the monoclinic space group $C2/c$, whereas **4** crystallizes with three molecules of acetonitrile per formula unit in the triclinic space group $P\bar{1}$. In both cases, the structure consists of six Fe atoms in a twisted boat conformation. The six Fe atoms are again distributed within two linked triangular $[Fe_3(\mu_3\text{-O})]$ units (Fe1−Fe2−Fe3 and Fe4−Fe5−Fe6) with a dihedral angle of 44.2° in **3** and 39.2° in **4**. A noncrystallographic mirror plane lies through atoms O3, O24, and O25 in **3,** and O2, O23, and O25 in **4**, and the molecules thus have virtual C_s symmetry. The central μ_3-oxide atom in each Fe_3 subunit is almost in the Fe_3 plane; in **3**, one lies 0.188 Å from the Fe1−Fe2−Fe3 plane, and the other 0.105 Å from the Fe4−Fe5−Fe6 plane. In **4**, the two oxide atoms are at very similar distances from their respective Fe_3 planes (average 0.186 Å). In contrast to **1** and **2**, the two sets of bridging ligands connecting the two Fe_3 units are not the same. One set comprises one μ-hydroxide group and two μ-carboxylate groups as in **1** and **2**, but the other set comprises one μ-carboxylate group and two μ-alkoxide groups from two nonchelating hep^- ligands (i.e., whose N atoms are not ligated to an Fe atom). The structure of each Fe_3 triangular unit in **3** and **4** is again scalene and similar to those in **1** and **2**. Fe1 and Fe2 are bridged by two μ-carboxylate groups, while Fe2 and Fe3 in **3** and Fe1 and Fe3 in **4** are bridged by one μ-carboxylate group and the

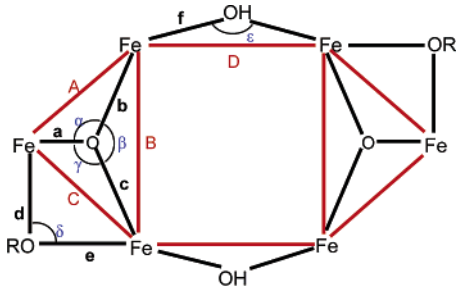

1 and **2**: *trans*

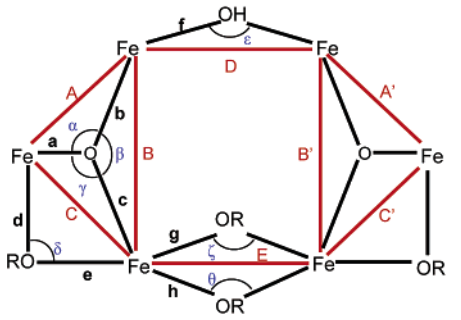

3 and **4**: *cis*

Figure 2. Diagrammatic scheme of the core structures of complexes **1**−**4**, and defining the distance and angle labels used in Table 2. Symmetry-equivalent quantities are not labeled.

μ-alkoxo group of a chelating hep^- ligand. There are again intramolecular hydrogen bonds across the central gap, this time between the oxygen atom of the bridging hydroxide group (O3 in **3**, O2 in **4**) and the oxygen atom of one of the alkoxide bridges (O25 in both **3** and **4**), with distances of 2.783(1) and 2.761(2) Å in **3** and **4**, respectively.

It is interesting that the conversion of **1** and **2** to **3** and **4**, respectively, by the incorporation of two extra hep^- groups, has not led to the latter being incorporated in a symmetric manner, but instead on the same side of the molecule.

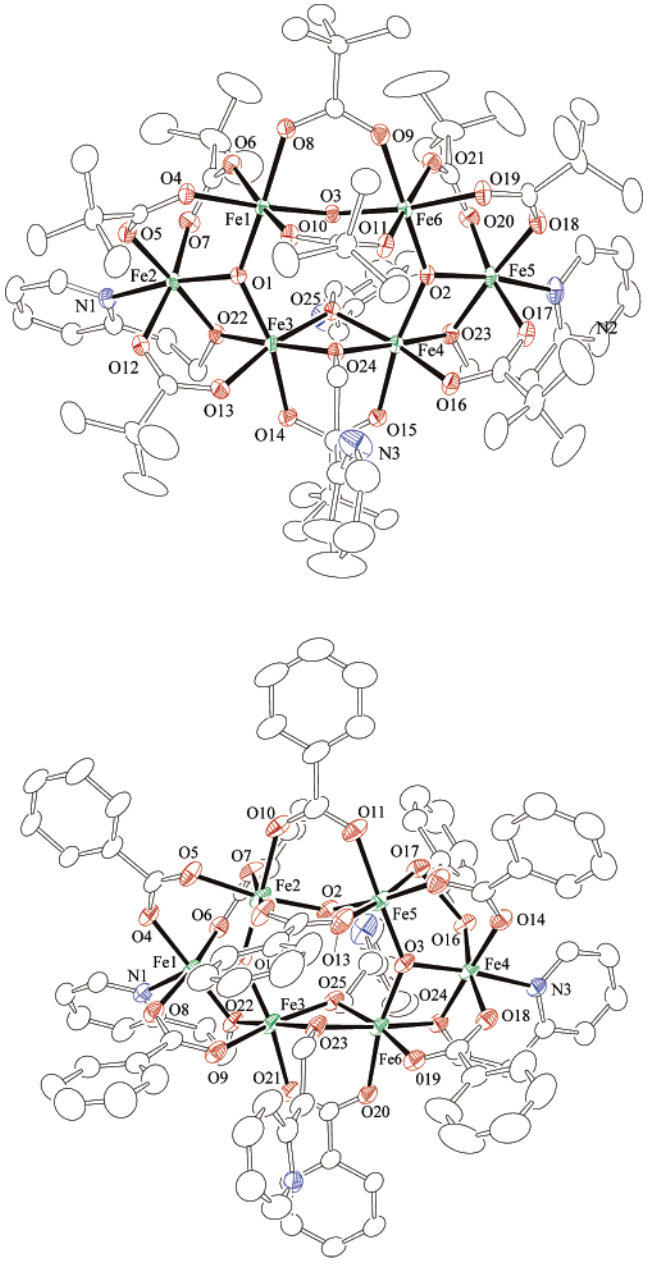

Figure 3. ORTEP representations of $[Fe_6O_2(OH)(O_2CBu^t)_9(hep)_4]$ (**3**) (top) and $[Fe_6O_2(OH)(O_2CPh)_9(hep)_4]$ (**4**) (bottom), with the atoms drawn at the 50% probability level. Hydrogen atoms have been omitted for clarity.

Nevertheless, this is likely the primary reason that the structures of **3** and **4** are distinctly different from those of **1** and **2** in a very important way: the two short, monatomically bridged Fe_2 pairs (Fe2Fe3 and Fe4Fe5 for **3**, and Fe1Fe3 and Fe4Fe6 for **4**) are now on the same side of the molecule, and the core topology of **3** and **4** is thus described as *cis*. There are no previously reported examples of Fe_6 compounds with this *cis* topology.

Magnetism Studies. Compounds 1 and 2. Variable-temperature, solid-state magnetic susceptibility measurements were performed on microcrystalline samples of **1** and **2** at 0.5 and 1.0 T, respectively, in the 2.0−300 K temperature range. The samples were restrained in eicosane to prevent torquing. The obtained data were very similar for both compounds and are shown in Figure 5 as effective magnetic

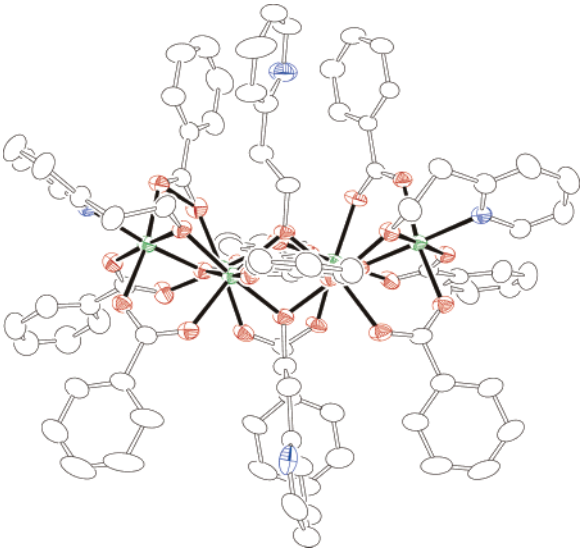

Figure 4. Side view of $[Fe_6O_2(OH)(O_2CPh)_9(hep)_4]$ (**4**) with the atoms drawn at the 50% probability level. Hydrogen atoms and solvent molecules have been omitted for clarity.

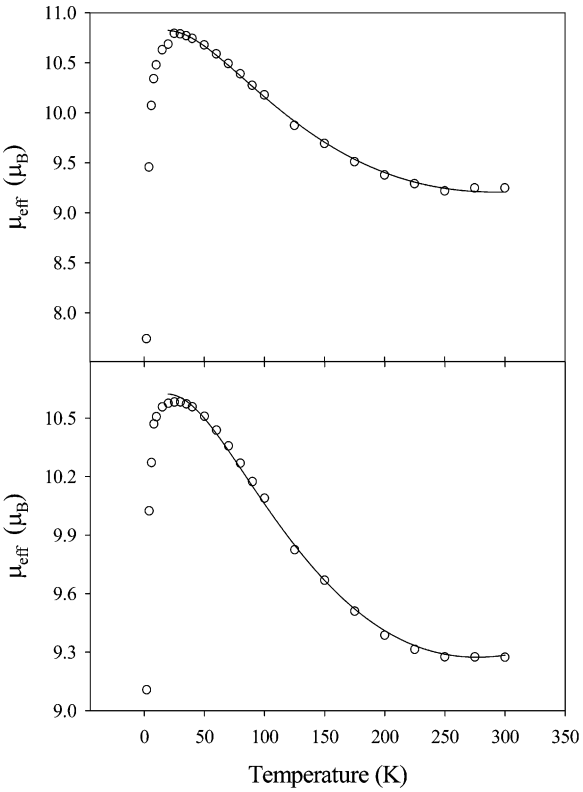

Figure 5. Plot of the effective magnetic moment per Fe_6 vs temperature for $[Fe_6O_2(OH)_2(O_2CBu^t)_{10}(hep)_2]$ (**1**) (top) and $[Fe_6O_2(OH)_2(O_2CPh)_{10}(hep)_2]$ (**2**) (bottom). The solid line corresponds to the theoretical fit (see the text for details).

moment (μ_{eff}) per Fe_6 versus T. The μ_{eff} at room temperature is 9.3 μ_B, below the spin-only ($g = 2$) value expected for six noninteracting Fe^{III} ions (14.49 μ_B), indicating the presence of antiferromagnetic interactions. The μ_{eff} gradually increases with decreasing temperature, reaching a plateau of 10.8 μ_B at 20 K for **1** and 10.6 μ_B at 30 K for **2**. These are very close to the spin-only value (10.95 μ_B) calculated for a system with an $S = 5$ ground state. The μ_{eff} drops sharply at the lowest temperatures, reaching a minimum of

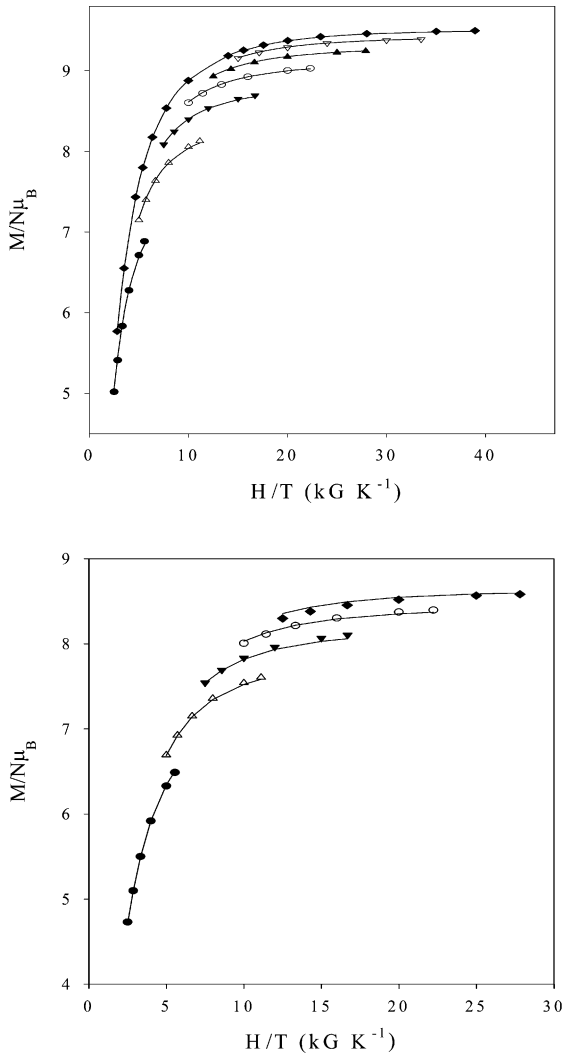

Figure 6. Plot of the reduced magnetization ($M/N\mu_B$) vs H/T for (top) complex **1** in applied fields of 1 (●), 2 (△), 3 (▼), 4 (○), 5 (▲), 6 (▽), and 7 (♦) T, and (bottom) for complex **2** in applied fields of 1 (●), 2 (△), 3 (▼), 4 (○), and 5 (♦) T. The solid lines are the fits of the data; see the text for the fitting parameters.

9.3 μ_B for **1** and 9.1 μ_B for **2** at 2.0 K, most likely due to zero-field splitting (ZFS) of the ground state, as well as weak intermolecular antiferromagnetic interactions.

In order to confirm the indication from the above data of an $S = 5$ ground state for **1** and **2**, variable-temperature and -field magnetization (M) data were collected on the same samples of **1** and **2**. Data were collected in the 1−7 T and 1.7−4.0 K field and temperature ranges. The obtained data are plotted as reduced magnetization ($M/N\mu_B$) versus H/T, where N is Avogadro's number, in Figure 6. Both plots display nonsuperimposed isofield lines characteristic of a system with significant zero-field splitting (ZFS). The saturation values of the reduced magnetization at the highest fields and the lowest temperatures are around 9 μ_B, slightly below the expected saturation value (10 μ_B) for a ground state with $S = 5$ and $g = 2$. The data were least-squares fit by diagonalizing the spin Hamiltonian matrix, including axial (D) and rhombic (E) ZFS terms and Zeeman interactions, assuming that g is isotropic and that only the ground state is populated at these temperatures, and calculating a full powder average of the magnetization. The method is described in more detail elsewhere.[20,21] The fits, shown as solid lines in Figure 6, gave $S = 5$, $g = 1.9550(5)$, $D = 0.458(3)$ cm^{-1}, and $E = \pm 0.046$ cm^{-1} for complex **1**, and $S = 5$, $g = 1.889(7)$, $D = 0.69(3)$ cm^{-1}, and $E \sim 0$ cm^{-1} for compound **2**. Alternative fits with different values of S were discarded because they gave unreasonable values of g.

The g versus D error surfaces for the fits for compounds **1** and **2** were calculated to assess whether the values found for g and D do indeed correspond to the global rather than local minima. There are actually two minima in both cases, one with a positive D value and the other with a negative one. This is as is typically found in such fits, which are not very sensitive to the sign of D. Nevertheless, the relative error of the fits for both compounds is smaller when $D > 0$. This fact, together with previously reported measurements of the magnetization relaxation behavior of **1** at very low temperatures,[6] which is consistent with $D > 0$, supports the conclusion that compounds **1** and **2** have the D values given above, both with $D > 0$.

Compounds 3 and 4. Variable-temperature, solid-state magnetic susceptibility measurements were performed on microcrystalline samples of **3** and **4** in a 1.0 T field in the 2.0−300 K temperature range. The samples were restrained in eicosane to prevent torquing. The data are plotted as μ_{eff} versus T in Figure 7. The μ_{eff} steadily decreases from 8.5 μ_B for **3** and 8.8 μ_B for **4** at 300 K to 1.4 μ_B and 0.8 μ_B at 2.0 K for **3** and **4**, respectively. As for **1** and **2**, the values at 300 K are much lower than that expected for a cluster of six noninteracting Fe^{III} ions with $g = 2$ (14.49 μ_B), again indicating the presence of predominantly antiferromagnetic exchange interactions. In contrast to **1** and **2**, however, the monotonically decreasing μ_{eff} with decreasing temperature and the resultant low value at 2.0 K are indicative of an $S = 0$ ground state for compounds **3** and **4**.

The magnetic studies thus establish that the two groups of compounds, **1**/**2** and **3**/**4**, have very different ground state spin values even though their structures are quite similar. This is a dramatic difference, corresponding to 10 unpaired electrons. The structures differ in only two significant ways: (i) the *cis* versus *trans* disposition of the two triangular Fe_3 units, and (ii) the change in the identity of two of the bridging ligands between the Fe_3 units. One or both of these differences could be the cause of the variation in S. Ultimately, the ground state spin must be dependent upon the various pairwise Fe_2 exchange interactions (J) in the molecule, since these will determine the alignment of the various spins in the molecule and thus its ground state S value. But the pairwise Fe_2 exchange (actually superexchange) interactions are primarily determined by the bridging ligands across that Fe_2 pair and the attendant metric parameters, and these are all essentially the same in **1**/**2** and **3**/**4** except for the one difference noted as ii. Therefore, it could possibly be that a major change in the J value at this

(20) Vermass, A.; Groeveld, W. L. *Chem. Phys. Lett.* **1984**, *27*, 583.
(21) Yoo, J.; Yamaguchi, A.; Nakano, M.; Krzystek, J.; Streib, W. E.; Brunel, L.-C.; Ishimoto, H.; Christou, G.; Hendrickson, D. N. *Inorg. Chem.* **2001**, *40*, 4604.

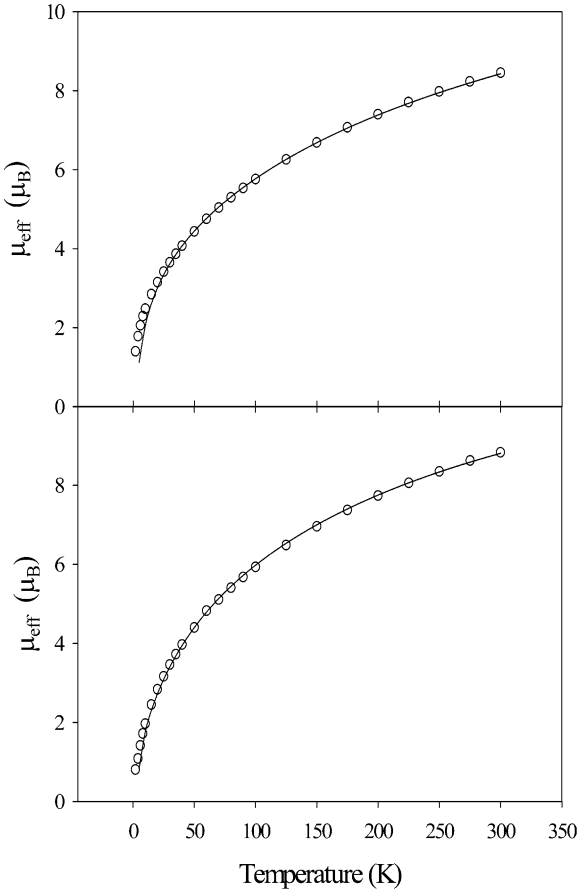

Figure 7. Plot of the effective magnetic moment per Fe_6 vs temperature for $[Fe_6O_2(OH)(O_2CBu^t)_9(hep)_4]$ (**3**) (top) and $[Fe_6O_2(OH)(O_2CPh)_9(hep)_4]$ (**4**) (bottom). The solid line corresponds to the theoretical fit (see the text for details).

one Fe_2 pair may be enough to dramatically alter somehow the spin alignments at these and adjacent Fe atoms and thus be the origin of the large change in *S*. Alternatively, although the pairwise *J* values are expected to be similar in the two types of molecule, the *cis* versus *trans* difference may be somehow leading to a major difference in the spin alignments and to different *S* values, especially since Fe_3 triangular units are present and these have long been recognized to be susceptible to spin frustration effects. In other words, differences in either the couplings between Fe_3 units (interunit couplings) or the couplings within Fe_3 units (intraunit couplings) could lead to the observed difference in spin. Or, of course, both these effects may be contributing to the observed difference. In any event, it is clear that if the large spin differences are to be explained in a quantitative manner rather than merely being qualitatively assigned as somehow due to the two identified structural differences, then a necessary first step must be to obtain reliable values for the various exchange constants in the molecules. For this reason, we carried out the calculations described below.

Semiempirical Calculations. Semiempirical calculations using the ZILSH method[7,11] were performed to analyze the exchange interactions underlying the magnetic properties observed for complexes **1**−**4**. These calculations take place in three stages. First, energies and spin couplings are computed for a set of UHF component wave functions using the INDO/S model of Zerner.[12,13] Estimates of the exchange constants (*J*) are then obtained from these quantities by simultaneous solution of eqs 2. In the second stage, the exchange constants are adjusted using the genetic algorithm fitting method to more closely reproduce the experimentally measured variable-temperature magnetic susceptibility of the complexes. In the third and final stage, the exchange constants found in the second stage are substituted into the Heisenberg spin Hamiltonian, which is diagonalized in a basis of spin components (eq 4) to yield the final energies and wave functions of the spin states. Results for each stage of the calculations are discussed in turn below.

Table 3. ZILSH Exchange Constants[a] and Spin Couplings[b] for Complexes **1**−4

parameter	**1**	**2**	**3**	**4**
J_{12}	−40.3	−39.0	−42.5	−40.9
J_{13}	−21.4	−15.9	−20.1	−22.1
J_{23}	−50.8	−55.6	−47.9	−49.0
J_{24}	−24.2	−28.5	−29.1	−31.3
J_{35}			−24.0	−20.1
J_{45}			−53.4	−48.0
J_{46}			−44.6	−42.8
J_{56}			−24.0	−20.3
$\langle \hat{S}_1^2 \rangle$	8.31	8.29	8.31	8.33
$\langle \hat{S}_2^2 \rangle$	8.33	8.29	8.32	8.30
$\langle \hat{S}_3^2 \rangle$	8.36	8.34	8.32	8.34
$\langle \hat{S}_4^2 \rangle$			8.27	8.34
$\langle \hat{S}_5^2 \rangle$			8.33	8.36
$\langle \hat{S}_6^2 \rangle$			8.31	8.31
$\langle \hat{S}_1 \cdot \hat{S}_2 \rangle$	−4.79	−4.76	−4.78	−4.78
$\langle \hat{S}_1 \cdot \hat{S}_3 \rangle$	4.79	4.77	4.77	4.79
$\langle \hat{S}_2 \cdot \hat{S}_3 \rangle$	−4.80	−4.77	−4.78	−4.77
$\langle \hat{S}_2 \cdot \hat{S}_4 \rangle$	−4.79	−4.77	−4.75	−4.77
$\langle \hat{S}_3 \cdot \hat{S}_5 \rangle$			−4.78	−4.80
$\langle \hat{S}_4 \cdot \hat{S}_5 \rangle$			−4.76	−4.80
$\langle \hat{S}_4 \cdot \hat{S}_6 \rangle$			−4.76	−4.79
$\langle \hat{S}_5 \cdot \hat{S}_6 \rangle$			4.77	4.79
$\langle S^2 \rangle$	40.66	46.22	16.43	22.09

[a] Exchange constants are in cm^{-1}; symmetry-related parameters are not included. [b] Obtained from the M = 5(UHF) approximations of the ground states of **1** and **2**, and from the M = 0(UHF) approximations of the ground states of **3** and **4**.

The exchange constants found for complexes **1**−**4** from the energies and spin couplings of UHF component wave functions are given in Table 3. All interactions are antiferromagnetic, as expected for high-spin Fe^{3+} (d^5) ions. The values obtained reflect the symmetry of the complexes; **1** and **2** have crystallographic inversion symmetry, so four unique exchange constants (J_A, J_B, J_C, and J_D for interactions A, B, C, and D in Figure 2) were obtained for these complexes. In contrast, **3** and **4** have lower crystallographic symmetry, resulting in distinct values for all eight nonzero exchange constants. There is, however, a virtual plane of symmetry relating the two triangular subunits, as can be seen by comparing J_A and $J_{A'}$ (e.g., −42.5 vs −44.6 cm^{-1} in complex **3**), J_C and $J_{C'}$ (−20.1 and −24.0 cm^{-1}), and J_B and $J_{B'}$ (−47.9 and −53.4 cm^{-1}). All exchange constants other than those given in Table 3 (and their symmetry-equivalent partners) were found to be zero. The nonzero values obtained for each interaction are similar in all four complexes, which is not surprising given their similar structures and ligands.

It is important to consider the spin couplings computed from the UHF wave functions in evaluating how accurate

the predicted exchange constants are. Values of the local spin moments $\langle \hat{S}_A^2 \rangle$ and spin couplings $\langle \hat{S}_A \cdot \hat{S}_B \rangle$ for single determinant approximations of the ground-state wave functions of complexes **1**−**4** are given in Table 3. As stated earlier, exchange constants extracted from single determinant wave functions are formally equal to those of the spin states of the system if the determinant wave functions are high spin eigenfunctions of the local spin operators $\hat{S}_A^2$. If that were the case, values of $S_A(S_A + 1) = 8.75$ would be obtained for high spin Fe^{3+} ions, which have spin quantum numbers of $^5/_2$. The values given in Table 3 are reasonably close to this for all four complexes. Another measure of how closely the exchange constants resemble those of the spin states is given by the expectation value of the total spin operator, $\langle \hat{S}^2 \rangle$. If the determinants were high-spin eigenfunctions of the local spin operators, this expectation value would be given by eq 3. Values found for the components described in Table 3 are similar to the values of 40 and 15 predicted by the equation.

One interesting contrast in Table 3 is that the expectation values of the total spin operator obtained for the complexes with $PhCO_2^-$ ligands (**2** and **4**) are significantly further from the values given by eq 3 than are those for the complexes with $Bu^tCO_2^-$ ligands (**1** and **3**). Although we have not examined this in detail, it appears that this discrepancy arises from differences in local spin expectation values for the carbon atoms on the substituent groups, rather than from any differences in local spins or spin couplings of the metal ions. This is supported by the results of Table 3, in which the local spins and spin couplings involving the metal ions are similar for all four complexes.

The results of the previous paragraph demonstrate that the error caused by using UHF components that are not formally high-spin eigenfunctions of local spin is reasonably small. It is important to note that the local spin expectation values in Table 3 are very similar for the $S = 0$ and $S = 5$ complexes. This indicates that the exchange constants found for all complexes should be of comparable accuracy despite the difference in spin. This is not generally true for spin-dependent quantities obtained from single determinant wave functions due to the so-called "spin contamination". It occurs in this case because spin contamination errors in the energies are exactly compensated for by spin contamination errors in the local spin couplings $\langle \hat{S}_A \cdot \hat{S}_B \rangle$. In other words, both the energy on the left side of eq 2 and the spin coupling on the right side of eq 2 are contaminated by a linear combination of higher spin states, with the same expansion coefficients on both sides. These then cancel, yielding uncontaminated values for the exchange constants. This is formally demonstrated, and thoroughly discussed, in ref 7.

There is some error inherent in the parametrization of the INDO/S method that would be present even if a basis of local spin eigenfunctions were used to obtain the exchange constants. In our previous experience,[7,11] exchange constants obtained from ZILSH provide a qualitatively correct description of exchange interactions in a complex, and correctly predict the ground state spin in most cases. However, ZILSH exchange constants typically do not closely reproduce

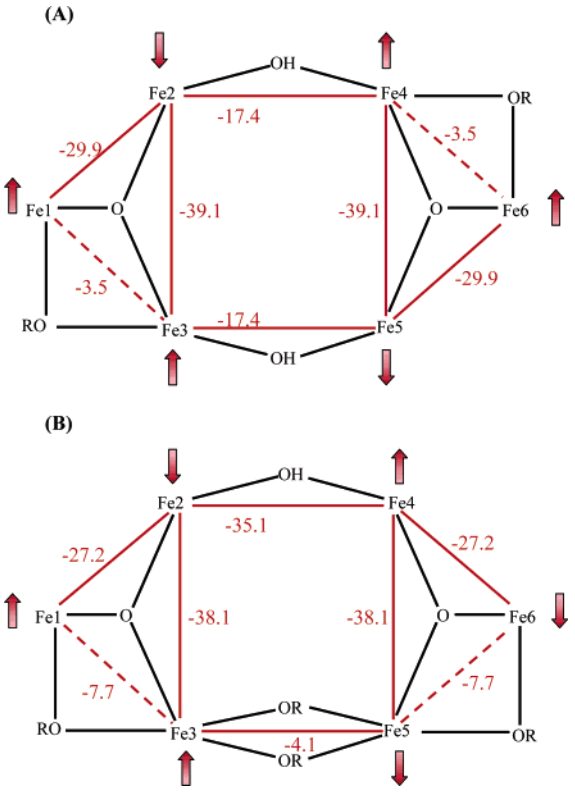

Figure 8. Schematic representation of the exchange interactions in complexes **1**−**4**. Frustrated interactions are indicated with dashed lines. (A) Complexes **1** and **2**, ground state $S = 5$. (B) Complexes **3** and **4**, ground state $S = 0$.

experimental magnetic susceptibility data in a quantitative sense. This was the case for the complexes considered here, so the ZILSH /genetic algorithm method was used to further refine the results.

The exchange constants calculated by ZILSH served as a valuable starting point for the susceptibility fits and provided reasonable models for fitting, with the constants that were found to be equivalent being set equal in the fits. Thus, four unique, nonzero exchange constants were allowed to vary in the fits for complexes **1** and **2** ($J_{12} = J_{56}$, $J_{13} = J_{46}$, $J_{23} = J_{45}$, and $J_{24} = J_{35}$; see Figure 8 for the numbering scheme), along with the g factor and the temperature independent paramagnetism (TIP). In complexes **3** and **4**, five independent values were used in the fits ($J_{12} = J_{46}$, $J_{13} = J_{56}$, $J_{23} = J_{45}$, J_{24}, and J_{35}) along with the g factor and the TIP. All parameters (J's, g, and TIP) were varied simultaneously to minimize the difference between calculated and experimental magnetic susceptibility at each temperature. The resulting exchange constants are given in Table 4, and the predicted magnetic susceptibilities are shown as the solid lines in Figure 5 (for **1** and **2**) and Figure 7 (for **3** and **4**).

The exchange constants obtained for complexes **1** and **2** agree well with values found by a fit for the analogous ($S = 5$) complex $[Fe_6O_2(OH)_2(O_2CCH_3)_{10}L_2]$,[18,19,22] with a *trans* topology, where L is an imidazole-based ligand with formula $C_{10}H_{13}N_4O^-$. In that work, values of -38 cm^{-1} were found

(22) Harvey, D. F.; Christmas, C. A.; McCusker, J. K.; Hagan, P. M.; Chadha, R. K.; Hendrickson, D. N. *Angew. Chem., Int. Ed. Engl.* **1991**, *30*, 598.

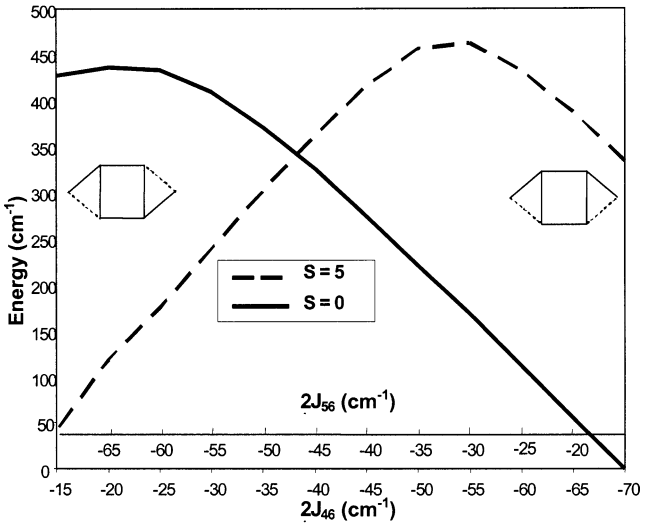

Figure 9. Plot of the energies of the lowest-energy $S = 5$ and $S = 0$ states for complex **1** versus J_{46} and J_{56} (see Figure 8 for numbering scheme).

for J_{12} and J_{23} (these parameters were artificially made equivalent in ref 23), -6 cm^{-1} for J_{13}, and -8 cm^{-1} for J_{24}, comparable to those found for **1** and **2** (Table 4). The exchange constants obtained for **3** and **4** are also rather similar to those found for **1** and **2**. This is as expected, because the corresponding pairwise Fe_2 exchange interactions have similar bridging ligands and bridging geometries. Also, the *g* factors given in Table 4 for **1** and **2** agree well with the values obtained by fitting the magnetization versus field data given above, 1.975 versus 1.955, and 1.939 versus 1.889, respectively.

Substitution of the exchange constants of Table 4 into the Heisenberg spin Hamiltonian (HSH) and diagonalization provide predictions for the ground state spins of the complexes. Compounds **1** and **2** are calculated to have ground state spins of $S = 5$, and **3** and **4** to have ground states of $S = 0$, in perfect agreement with the experimental data discussed in the previous section. The ground-state wave functions obtained for **1** and **2** are described in Table 5. They are dominated by a single component, $|\uparrow\downarrow\uparrow\uparrow\downarrow\uparrow\rangle$, where the arrows indicate $M_A = \pm 5/2$, using the numbering scheme of Figure 8. In both complexes, this component comprises almost half of the ground state wave function. The expectation values of M_A found in these ground states reflect the same alignment of spins, but with magnitudes reduced from $\pm 5/2$ by the admixture of other components into the wave function. In these complexes with $S = 5$ ground states, both the leading contributions to the wave function and the local *z*-components provide a clear picture of the spin alignments in the ground state.

In contrast, for **3** and **4** the leading contributions are made by components representing less than 12% of the wave function, and the local *z*-components of spin M_A are zero. This is typical for singlet states. In these cases, the average spin couplings $\langle \hat{S}_A \cdot \hat{S}_B \rangle$ computed from the spin state wave function give a better indication of the spin alignments. Positive values of $\langle \hat{S}_A \cdot \hat{S}_B \rangle$ indicate parallel alignment, while negative values indicate antiparallel alignment. These expectation values are given for all nonzero interactions in the ground states of the four complexes in Table 6. They show that the spins of Fe_1 and Fe_3 are aligned parallel in all four complexes. The spins of Fe_4 and Fe_6 are aligned parallel in complexes **1** and **2**, while the spins of Fe_5 and Fe_6 are aligned parallel in **3** and **4**. As discussed in the next section, this difference determines the spin of the ground state of each complex.

Spin Frustration and the Ground State Spins of Complexes 1−4. The pairwise Fe_2 exchange constants given in Table 4 for complexes **1**−**4** show that all nonzero interactions in these complexes are antiferromagnetic. Each pair of interacting spins would thus align antiparallel in the absence of other interactions. Nevertheless, as can be seen in Figure 8, two pairs of interacting spins are aligned parallel in each complex in the ground state. The reason for this is spin frustration. Spin frustration can be defined in a general sense as the presence of competing antiferromagnetic exchange interactions.[5,23] When these are all of comparable strength, a balance is reached, and the ground state spin alignments become very sensitive to the relative magnitudes of the competing interactions. In contrast, when the competing interactions are of significantly different strengths, then the strongest ones prevail and align the spins they control antiparallel, whereas the weakest ones are totally frustrated. This leads to the situation where the interaction between a pair of metals may be antiferromagnetic but the spins on these metals will nevertheless be aligned parallel due to the influence of stronger exchange interactions in adjacent metal pairs. Such effects are commonly encountered in a triangular arrangement of three antiferromagnetically coupled metal ions. In this topology, it is impossible for each of the spins to be aligned antiparallel to both of its neighbors.

Complexes **1**−**4** contain an Fe_6 topology that comprises two Fe_3 triangular units, and because the calculations described have determined that all the interactions are antiferromagnetic, spin frustration effects can be expected. Indeed, spin frustration has previously been invoked to explain the magnetic properties of other Fe_6 compounds with the *trans* topology of **1** and **2** and a resulting $S = 5$ ground state.[18,19] In the discussion below, we show that the results of our calculations confirm how the $S = 5$ ground state arises for the *trans* topology, but more importantly, it also becomes clear why the newly discovered *cis* topology of **3** and **4** naturally leads to an $S = 0$ ground state. As will be seen, the answer lies in the differing relative distribution of totally frustrated exchange pathways in the *cis* versus *trans* forms.

The significant difference in strength between exchange constants in **1**−**4** leads to some interactions being totally frustrated. The distribution of frustrated pathways and the resulting spin alignments are shown in Figure 8, where the frustrated pathways are denoted by dashed lines. The

(23) (a) Wang, S.; Tsai, H. L.; Streib, W. E.; Christou, G.; Hendrickson, D. N. *J. Chem. Soc., Chem. Commun.* **1992**, *9*, 677. (b) McCusker, J. K.; Jang, H. G.; Wang, S.; Christou, G.; Hendrickson, D. N. *Inorg. Chem.* **1992**, *31*, 1874. (c) Ribas, J.; Albela, B.; Stoeckli-Evans, H.; Christou, G. *Inorg. Chem.* **1997**, *36*, 2352. (d) Khan, O. *Chem. Phys. Lett.* **1997**, *265*, 109.

Table 4. Exchange Constants for **1**−**4** Obtained Using the Genetic Algorithm Method[a,b]

parameter[c]	**1**	**2**	**3**	**4**
J_{12}	−34.0 (−40.3)	−29.9 (−39.0)	−30.8 (−42.5, −44.6)	−27.2 (−40.9, −42.8)
J_{13}	−7.5 (−21.4)	−3.5 (−15.9)	−16.1 (−20.1, −24.0)	−7.7 (−20.3, −22.1)
J_{23}	−46.9 (−50.8)	−39.1 (−55.6)	−32.9 (−47.9, −53.4)	−38.1 (−48.0, −49.0)
J_{24}	−17.0 (−24.2)	−17.4 (−28.5)	−21.0 (−29.1)	−35.1 (−31.3)
J_{35}			−7.5 (−24.0)	−4.1 (−20.1)
g	1.975	1.939	1.996	1.990
TIP	1165×10^{-6}	982×10^{-6}	1134×10^{-6}	915×10^{-6}
σ[d]	0.05	0.05	0.03	0.05

[a] Numbering scheme as in Figure 8; the numbers in parentheses are those obtained from the ZILSH calculation (Table 3). [b] Parameters assumed to be symmetry-equivalent are not included. [c] J values in cm^{-1}; TIP in $cm^3\ mol^{-1}$. [d] Sum of differences between experimental and calculated values of $\chi_m T$ over all temperatures.

Table 5. Ground State Properties of **1**−**4** Computed with the Heisenberg Spin Hamiltonian[a,b]

compd	S	leading contribution[c] (weight)	$2\mathbf{S}_z$ (Fe_1)	$2\mathbf{S}_z$ (Fe_2)	$2\mathbf{S}_z$ (Fe_3)	$2\mathbf{S}_z$ (Fe_4)	$2\mathbf{S}_z$ (Fe_5)	$2\mathbf{S}_z$ (Fe_6)
1	5	$\|\uparrow\downarrow\uparrow\uparrow\downarrow\uparrow\rangle$ (0.439)	4.63	−3.98	4.35	4.35	−3.98	4.63
2	5	$\|\uparrow\downarrow\uparrow\uparrow\downarrow\uparrow\rangle$ (0.452)	4.63	−4.01	4.39	4.39	−4.01	4.63

[a] Numbering scheme as in Figure 8. [b] Exchange constants listed in Table 4 were used in all cases. [c] Format $|123456\rangle$.

Table 6. Exchange Constants (J), Average Spin Couplings ($\langle \hat{S}_A \cdot \hat{S}_B \rangle$), and Contributions to the Total Energy (ΔE) for the Ground States of **1**−**4**[a]

	1			**2**			**3**			**4**		
	J[b]	$\langle \hat{S}_A \cdot \hat{S}_B \rangle$	ΔE[c]	J[b]	$\langle \hat{S}_A \cdot \hat{S}_B \rangle$	ΔE[c]	J[b]	$\langle \hat{S}_A \cdot \hat{S}_B \rangle$	ΔE[c]	J[b]	$\langle \hat{S}_A \cdot \hat{S}_B \rangle$	ΔE[c]
Fe_1-Fe_2	−34.0	−7.13	−484.8	−29.9	−7.16	−428.3	−30.8	−7.17	−441.6	−27.2	−7.09	−386.0
Fe_1-Fe_3	−7.5	6.16	92.4	−3.5	6.16	43.1	−16.1	5.34	171.9	−7.7	6.21	95.7
Fe_2-Fe_3	−46.9	−7.47	−700.7	−39.1	−7.38	−576.9	−32.9	−7.11	−467.6	−38.1	−7.44	−566.8
Fe_2-Fe_4	−17.0	−6.17	−209.8	−17.4	−6.34	−220.7	−21.0	−6.15	−258.3	−35.1	−6.54	−459.4
Fe_3-Fe_5							−7.5	−7.57	−113.6	−4.1	−6.92	−56.7

[a] $\Delta E = -2J_{AB}\langle \hat{S}_A \cdot \hat{S}_B \rangle$. Numbering scheme as in Figure 8. [b] cm^{-1}. [c] cm^{-1}.

frustrated interactions are, of course, those with the weakest exchange constants, and they are overpowered by the other, stronger interactions. Although all interactions are antiferromagnetic in these Fe^{3+} complexes, the frustrated pathways are readily identified as those with positive average spin couplings (Table 6): Thus, the Fe1−Fe3 and Fe4−Fe6 pathways are frustrated in complexes **1** and **2**, and the Fe1−Fe3 and Fe5−Fe6 pathways are frustrated in **3** and **4**.

Now it can easily be seen that the *trans* and *cis* topologies will lead to $S = 5$ and $S = 0$ ground states for **1**/**2** and **3**/**4**, respectively, because they will determine the relative disposition of the frustrated pathways. In **1** and **2**, the frustrated pathways are Fe1/Fe3 and Fe4/Fe6 (Figure 8A), which are disposed *trans* in the molecule and thus are separated by Fe2 and Fe5, with which they couple antiferromagnetically and thus align their spins antiparallel. But as a result, the two separate pairs of parallel-aligned spins in the frustrated pathways are mutually parallel, and the *trans* molecule's total spin is therefore $S = 10 - 5 = 5$. In contrast, the frustrated pathways in **3** and **4** are Fe1/Fe3 and Fe5/Fe6 (Figure 8B), and they are adjacent. As a result, the spins of Fe3 and Fe5 directly couple and align antiparallel, and the two pairs of parallel-aligned spins in the frustrated pathways are consequently mutually antiparallel. Since the spins Fe2 and Fe4 are also aligned antiparallel, the *cis* molecule's total spin is $S = {}^{15}/_2 - {}^{15}/_2 = 0$. Thus, the calculated ground state S is directly determined by the *trans* ($S = 5$) or *cis* ($S = 0$) relative disposition of the two frustrated pairs, in perfect agreement with the experimental measurements described above.

The alternative hypothesis to explain the difference in ground state spins of the *cis* and *trans* forms given above was that variations in the couplings between the two triangular Fe_3O units (interunit couplings) lead to the spin reversal. In such a model, each Fe_3O unit would be considered to have a total spin of ${}^5/_2$, and these spins would then couple to give states with total spins ranging from 0 to 5. Variations in the interunit couplings could then lead to the observed reversal of spin. While there is considerable variation in the exchange constants found for the interunit pathways in the four complexes (Table 6), two important points make this alternative explanation unlikely. First, the ground state spins in complexes **1**−**4** do not change when the exchange constants for the interunit pathways are allowed to vary over wide ranges of values. For complex **1**, for example, the interunit pathways both have $J = -17.0\ cm^{-1}$ in the ground state. Even if these values are reduced to $J = -0.05\ cm^{-1}$ or increased to $-100\ cm^{-1}$, the ground state still has $S = 5$. A similar result holds for complexes **3** and **4** with singlet ground states: as long as the interunit couplings are antiferromagnetic, singlet ground states are obtained regardless of the magnitude of the interunit exchange constants. It is thus unlikely that variations in the values of these exchange constants between the various complexes could lead to the spin reversal.

The second point in favor of the *cis*−*trans* hypothesis is based on similar reasoning involving the couplings within the triangular Fe_3O units. It is quite easy to demonstrate that the spin reversal occurs as the frustrated pathways change from *cis* to *trans*, by allowing the exchange constants in one

Fe_3O unit to vary. For complex **1**, the frustrated pathways J_{13} and J_{46} (-7.5 cm^{-1}; see Figure 8 for numbering scheme) are in the *trans* relationship, as are the more strongly coupled pathways J_{12} and J_{56} (-34 cm^{-1}). The ground-state spin is then $S = 5$. If, hypothetically, these values were switched on one side of the complex (J_{46} was -34 cm^{-1} and J_{56} was -7.5 cm^{-1}), then the frustrated pathways would be in the *cis* relationship. These switched values lead to a ground state spin of $S = 0$.

A plot of the energies of the $S = 5$ and $S = 0$ states versus J_{46} and J_{56} for complex **1** (Figure 9) clearly shows how the ground state spin changes as the frustrated pathways switch from *trans* to *cis*. At the left side of the plot, $J_{46} = -7.5$ cm^{-1} and $J_{56} = -34$ cm^{-1}, the frustrated pathways are *trans*, and the ground state is $S = 5$ by a considerable margin. At the right side of the plot, $J_{46} = -34$ cm^{-1}, $J_{56} = -7.5$ cm^{-1}, the frustrated pathways are *cis*, and the ground state is $S = 0$. The cartoons at each side of the figure illustrate these extremes by showing the frustrated pathways as dashed lines. Moving from left to right on the plot, the spin reversal occurs as J_{46} becomes larger than J_{56}, and the pathway that is frustrated in the ground state goes from J_{46} to J_{56}. (Between the two extremes, the identities of the $S = 0$ and $S = 5$ states were established by monitoring the values of $\langle \hat{S}_A \cdot \hat{S}_B \rangle$ for different values of J_{46} and J_{56}. In particular, these quantities conclusively indicate which pathway is frustrated.) This convincingly demonstrates that the spin reversal is indeed occurring because of the arrangement of frustrated pathways, either *cis* or *trans*.

As mentioned earlier, the spin coupling value $\langle \hat{S}_A \cdot \hat{S}_B \rangle$ is useful for analyzing spin frustration effects because it represents the actual alignment of the spins of metal centers A and B in the spin state. It is positive and negative for parallel and antiparallel alignments, respectively. The J value merely reflects the preferred alignment. If $\langle \hat{S}_A \cdot \hat{S}_B \rangle$ and J_{AB} differ in sign, the A−B pathway is frustrated. In a more quantitative sense, the product $-2J_{AB}\langle \hat{S}_A \cdot \hat{S}_B \rangle$ (referred to as ΔE in Table 6) represents the contribution made by the A−B pathway to the total energy of the spin state (see eq 2). The interaction of spins through frustrated pathways thus increases the total energy of the system. With this definition, it is clear why complete spin frustration occurs in pathways with the weakest exchange constants: the energy is increased only slightly by the frustrated interaction, which is more than compensated for by larger decreases in the energy in other pathways with stronger exchange constants. This is demonstrated by the values of ΔE in Table 6, where the positive contributions from the frustrated pathways are much smaller than the negative contributions from other pathways.

The quantity ΔE provides a quantitative measure of which pathways stabilize the $S = 5$ state below the $S = 0$ state in complexes **1** and **2**, and vice versa for complexes **3** and **4**. In complex **1**, for example, the values of ΔE given in Table 6 for the $S = 5$ ground state indicate a total energy of -2606 cm^{-1} for this state (considering all symmetry-equivalent pathways). Of this total, -2186 cm^{-1} is contributed by the intraunit pathways (those within Fe_3O subunits, i.e., 1−2, 1−3, 2−3, 4−5, 4−6, and 5−6 in Figure 8), while -420 cm^{-1} is contributed by the interunit pathways (2−4 and 3−5). Table 7 lists the energies of the $S = 5$ and $S = 0$ states of complexes **1** (ground state $S = 5$) and **3** (ground state $S = 0$), along with contributions from the interunit and intraunit pathways. For complex **1**, it can be seen by subtracting the energies in Table 7 that the $S = 5$ state is stabilized relative to the $S = 0$ state by 461 cm^{-1} (given as $E_{S=5} - E_{S=0}$ in the table). Similarly, it can be seen that the intraunit pathways contribute 374 cm^{-1} to this stabilization (given as $\Delta(\Delta E)$, intraunit pathways in Table 7), while the interunit pathways contribute only 87 cm^{-1}.

Table 7. Energies of the $S = 5$ and $S = 0$ States of Complexes **1** and **3**, along with Contributions from Interunit and Intraunit Coupling Pathways[a]

state	quantity	complex **1**	complex **3**
$S = 5$	total energy (cm^{-1})	−2606	−1605
	ΔE, intraunit pathways (cm^{-1})	−2186	−1292
	ΔE, interunit pathways (cm^{-1})	−420	−314
$S = 0$	total energy (cm^{-1})	−2145	−1845
	ΔE, intraunit pathways (cm^{-1})	−1812	−1474
	ΔE, interunit pathways (cm^{-1})	−333	−372
–	$E_{S=5} - E_{S=0}$	−461	+240
–	$\Delta(\Delta E)$, $S = 5$ to $S = 0$ intraunit pathways	−374	+182
–	$\Delta(\Delta E)$, $S = 5$ to $S = 0$ interunit pathways	−87	+58

[a] See text for details.

Turning now to complex **3**, in this case the $S = 0$ state is the ground state, and is stabilized relative to the $S = 5$ state by 240 cm^{-1}. The intraunit pathways contribute 182 cm^{-1} to this total, while the interunit pathways contribute only 58 cm^{-1}. In both cases, it is apparent that while the interunit pathways do make small contributions to the stabilization energy, the primary contributions are made by the intraunit pathways. Since the only topological difference between the intraunit couplings in the $S = 5$ and $S = 0$ complexes is the topology of frustrated pathways, either *cis* or *trans*, this must then be the primary factor determining which state is more stable.

Magnetostructural Relationships. The above discussion has successfully rationalized the variation of the spins of the *trans* and *cis* Fe_6 core "isomers" based on the exchange constants. It is also important to consider the relationship between them and the structural parameters that determine their magnitude. Such a correlation would be useful for rationalizing observed magnetic properties of polynuclear complexes, and it could also assist in the deliberate synthesis of complexes with desirable magnetic properties (e.g., large spin ground states). Most attempts to date to establish magnetostructural correlations have focused on dinuclear systems, including hydroxide-bridged dicopper(II)[24] and dichromium(III)[25] complexes, oxide-bridged dimanganese(IV) complexes,[26] phenoxide-bridged dinickel(II) complexes,[27] and

(24) Handa, M.; Koga, N.; Kida, S. *Bull. Chem. Soc. Jpn*. **1988**, *61*, 3853.
(25) Thompson, L. K.; Mandal, S. K.; Tandon, S. S.; Bridson, J. N.; Park, M. K. *Inorg. Chem.* **1996**, *35*, 3117.
(26) Law, N. A.; Kampf, J. W.; Pecoraro, V. L. *Inorg. Chim. Acta* **2000**, *297*, 252.

oxide- hydroxide-, and alkoxide-bridged diiron(III) complexes.[28−34] In all cases, empirical or semiempirical relationships have been established between the exchange constant and the M−O−M angles or M−O bond lengths in the bridges.

Focusing now on the diferric complexes, Gorun and Lippard reported an exponential relationship between the exchange constant and a parameter related to Fe−O distances in oxide-bridged complexes.[28] The Fe−O−Fe angle was found to have only a second-order effect, a conclusion supported by ab initio calculations on $Cl_3Fe-O-FeCl_3$.[29] Weihe and Güdel[30] used a formulation based on the angular overlap model (AOM) to derive an expression for J as a function of both the Fe−O−Fe angle (φ) and the Fe−O distance (r) (eq 8).

$$J = A(B + C\cos\varphi + \cos^2\varphi)\exp(Dr) \qquad (8)$$

A fit to experimental data for a number of oxide-bridged diiron(III) complexes indicated that the magnetic interaction decreases when the Fe−O distance increases or when the Fe−O−Fe angle increases. Other, less extensive studies have also shown some dependence on angle.[31−33] More recently, Werner et al. studied the previously reported correlations in an extensive group of hydroxide-, alkoxide-, and phenoxide-bridged iron (III) dimers.[34] They applied both the exponential model of Gorun and Lippard[28] and eq 8. These authors concluded that angular dependence is small.

Despite the extensive literature devoted to magnetostructural correlations in dinuclear iron(III) compounds, very little has been reported on polynuclear complexes. The four Fe_6 compounds presented in this work provide sufficient independent exchange constants to allow a statistically meaningful magnetostructural correlation to be obtained for diferric units within polynuclear topologies. Tables 2 and 4 list the relevant structural and magnetic data. In a first attempt to correlate the magnetic and structural parameters, we employed an exponential expression similar to that of Gorun and Lippard.[28] The regression error obtained for a fit of the data using this expression was extremely large ($r = 0.70$). A closer examination of the parameters in Table 2, however, reveals a distinct relationship between the Fe−O−Fe angle and the coupling constant, in contrast to what was observed for dinuclear complexes. This is clearly displayed by Figure 10. In view of this, we next considered eq 8 as a model that includes both a radial and angular dependence.

The parameters of eq 8 that yield the minimum least-squares error are $A = 2 \times 10^7$ cm^{-1}, $B = 0.2$, $C = -1$, and

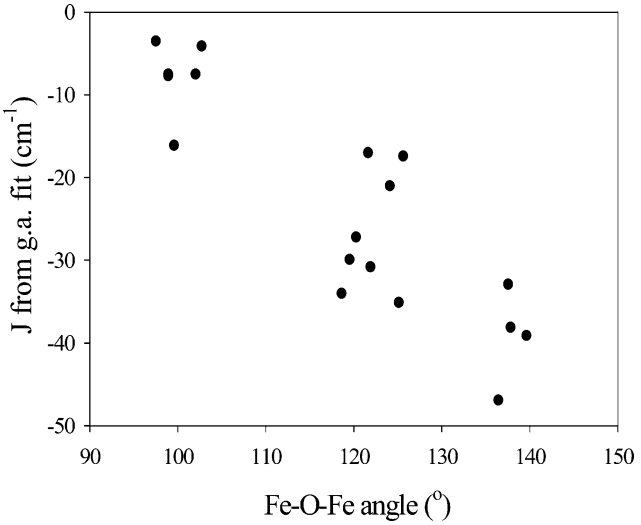

Figure 10. Plot of the exchange coupling constants (J) determined by the genetic algorithm fit of the ZILSH values vs the widest corresponding Fe−O−Fe angle.

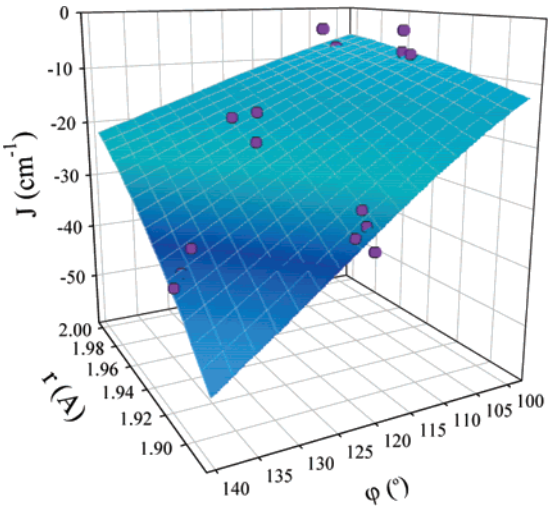

Figure 11. Three-dimensional surface plot of the angular and radial dependence of the exchange coupling constants (J). The surface has been generated by use of the expression $J = A(B + C\cos\phi + \cos^2\phi)\exp(Dr)$ with the parameters A, B, C, and D given in the text. J values obtained by the ZILSH-genetic algorithm fit are represented by dots.

$D = -7$ Å^{-1}. Whenever more than one bridge was present, the best results were obtained by employing the average distance for the shortest Fe−O bridge, which in all cases corresponds also to the one with a widest Fe−O−Fe angle. The results of the fit are shown in Figures 11 and 12. Figure 11 shows the three-dimensional surface representing the J values for every combination of Fe−O−Fe angle (φ) and Fe−O distance (r) as predicted from the correlation, together with the experimental values. A plot comparing the predicted and experimental J values of **1**−**4** is presented in Figure 12. The quality of the fit is very high, with a regression coefficient (r) of 0.94, whereas the same parameter for Weihe and Güdel's results for dinuclear complexes was 0.82.[30]

The picture that emerges for these hexanuclear complexes is that there is clearly both a radial and an angular dependence of the exchange constant. The exchange becomes more strongly antiferromagnetic (i.e., J has a larger negative value) as the Fe−O distance decreases and as the Fe−O−

(27) Nanda, K. K.; Thompson, L. K.; Bridson, J. N.; Nag, K. *J. Chem. Soc., Chem. Commun.* **1994**, 1337.
(28) Gorun, S. M.; Lippard, S. J. *Inorg. Chem.* **1991**, *30*, 1625.
(29) Hart, J. R.; Rapper, A. K.; Gorun, S. M.; Upton, T. H. *Inorg. Chem.* **1992**, *31*, 5254.
(30) Weihe, H.; Güdel, H. U. *J. Am. Chem. Soc.* **1997**, *119*, 6539.
(31) Gerloch, M.; Towl, A. D. C. *J. Chem. Soc. A* **1969**, 2850.
(32) Mukherjee, R. N.; Stack, T. D. P.; Holm, R. H. *J. Am. Chem. Soc.* **1988**, *110*, 1850.
(33) Le Gall, F.; Fabrizi de Biani, F.; Caneschi, A.; Cinelli, P.; Cornia, A.; Fabretti, A. C.; Gatteschi, D. *Inorg. Chim. Acta* **1997**, *262*, 123.
(34) Werner, R.; Ostrovsky, S.; Griesar, K.; Haase, W. *Inorg. Chim. Acta* **2001**, *326*, 78.

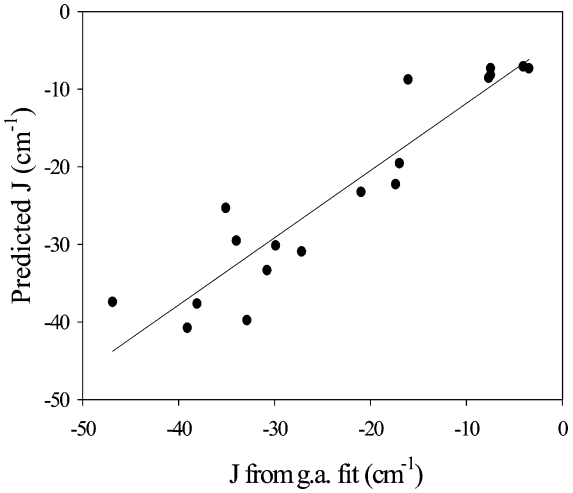

Figure 12. Plot of the *J* values obtained by the ZILSH-genetic algorithm fit versus the *J* values obtained from the magnetostructural correlation described in the text. The line $y = ax + b$ drawn is the best fit through the points ($a = 0.866$, $b = -3.16$). The correlation coefficient *r* is 0.94.

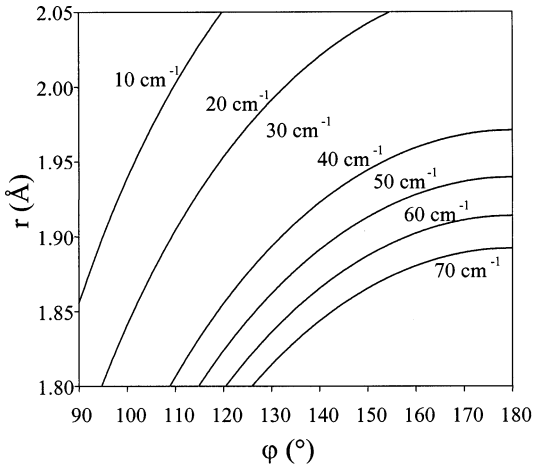

Figure 13. Iso-*J* curves (curves with the same value of exchange coupling constant *J*) for different combinations of Fe−O−Fe angle (φ) and average Fe−O distance (*r*).

Fe angle increases. This behavior is illustrated in Figure 13, which is a two-dimensional projection of the surface in Figure 11 showing the iso-*J* lines (lines of constant value of *J*) as a function of *r* and φ. It can be seen that the angular dependence is accentuated as *r* decreases, and the radial dependence is more important at wider angles. While the observation of a radial dependence was expected and is in accord with previous studies on dinuclear iron(III) compounds, the strong angular dependence is surprising and unprecedented.

The relative insensitivity of *J* to the Fe−O−Fe bridging angle in dinuclear compounds is thought to arise from the isotropic d-electron distribution of a high spin d^5 ion, which eliminates any angular dependence. Every Fe^{3+} ion in a dinuclear complex uses different d-orbitals to establish interactions with different angular dependencies. When the angle changes, these dependencies compensate each other so that no significant net angular dependence is observed; any decrease in overlap involving one 3d orbital is compensated by increases involving other 3d orbitals. In the case of polynuclear compounds, the situation is much more complex. Every metal center and its orbitals are involved in interactions with more than one other ion, and this will likely prevent the kind of compensation mentioned above and thus allow an angular dependence of *J* to be manifested. It is worth noting that our results agree with the predictions of Gerloch et al.[31] They showed that all possible exchange interactions between two iron(III) ions would lead to antiferromagnetism except for a ferromagnetic contribution that arises from an exchange interaction through two orthogonal orbitals in the bridging atom. This ferromagnetic contribution is operative when the angle approaches 90° and could be contributing to the results we observe.

Conclusions

Treatment of the trinuclear compounds $[Fe_3O(O_2CR)_6(hep)_3]^{0,+}$ (R = Bu^t, Ph) with 3 equiv of hepH represents a convenient route to the hexanuclear compounds $[Fe_6O_2(OH)_2(O_2CR)_{10}(hep)_2]$ (R = ^{t}Bu (**1**), Ph(**2**)) with a previously observed *trans* topology. The reaction of preformed **1** and **2** with an excess of hepH yields the structurally related hexanuclear compounds $[Fe_6O_2(OH)(O_2CR)_9(hep)_4]$ (R = ^{t}Bu (**3**), Ph(**4**)), with an unprecedented *cis* topology. This transformation can be reversed by recrystallization from acetonitrile. Both types of complexes contain two triangular $[Fe_3(\mu_3\text{-}O)(O_2CPh)_3(hep)]^{+3}$ units connected at two of their apices. However, **1** and **2** differ slightly from **3** and **4** in the means by which the two Fe_3 units are linked together, in either a *trans* or *cis* arrangement, which results in dramatically different magnetic properties. Magnetic data show **1** and **2** to have an $S = 5$ ground state and positive zero-field splitting, whereas **3** and **4** are diamagnetic. This large variation of 10 unpaired electrons in the net *S* values stresses the sensitivity of the magnetic properties of these polynuclear species to relatively small structural variations.

The semiempirical molecular orbital method ZILSH has proven a particularly useful way to explain the differences observed. It has allowed good estimates of the exchange constants of each complex to be obtained, which can then be refined by a genetic algorithm fit to the experimental variable-temperature magnetic susceptibility data. It has allowed also the spin topology of the ground states to be determined. As a result, it has been established that the large difference of 10 unpaired electrons in the net spin of the ground states is the direct consequence of a single structural difference between the two types of complexes, the relative disposition of the two completely frustrated exchange pathways whose spins are forced to align parallel by other, stronger interactions. It is thus now perfectly clear why the *trans* and *cis* Fe_6 topological isomers lead to $S = 5$ and $S = 0$ ground states, respectively. It is worth emphasizing that the change in one of the bridging sets linking the two Fe_3 subunits within the Fe_6 structure, from $[(\mu\text{-}OH)(\mu\text{-}O_2CR)_2]$ in **1** and **2** (e.g., between Fe3 and Fe2′ in Figure 1) to $[(\mu\text{-}OR)_2(\mu\text{-}O2CR]$ in **3** and **4** (e.g., between Fe3 and Fe4 in Figure 3, top), does significantly change the *J* value within this Fe_2 pair, but that the latter per se is not the cause of the change in ground state *S*. In both cases, the *J* value at this position is negative (antiferromagnetic); this exchange

interaction is not competing with any other to align spins, and thus, the magnitude of *J* at this position is irrelevant to the spin frustration effects that determine the ground state. Nevertheless, this change in bridging ligands is indirectly crucial to the change in *S* because it very much appears that it causes the structural change from *trans* to *cis* topology that then does affect the ground state spin value.

Finally, a magnetostructural correlation has been established that relates the exchange interaction constants *J* with both the average Fe−O distance and the Fe−O−Fe angle through the shortest Fe−O−Fe bridge. In effect, this correlation is for Fe_2 pairs whose Fe atoms are also involved in additional bridging interactions with other Fe atoms. The correlation indicates that the antiferromagnetic interaction is stronger as the Fe−O−Fe angle increases and the Fe−O distance decreases, which is qualitatively logical. Despite the complexity of the Fe_6 molecules considered, the variation of the exchange constants can be correlated to only one of the exchange pathways between each pair of related ions, the one with the larger angle and shortest length. Moreover, the identity of the bridge (O^{2-}, HO^-, or RO^-) does not itself affect the interaction, other than its influence on the corresponding bond distances and angles. We feel this correlation should prove useful in the future, both for hindsight rationalization of experimentally determined ground states, and for prediction of the exchange constants and ground states of new polynuclear complexes. The latter could also be particularly useful for predicting the position of the weakest interactions, which are likely to be totally frustrated, and thus predicting how the ground state would vary with isomeric changes in the Fe_x topology, as we did in the present work for **1**−**4**. This is one of the most difficult questions to answer in polynuclear complexes, and yet extremely important especially in the directed design of species with desirable magnetic properties.

Acknowledgment. This work was supported by the National Science Foundation.

Supporting Information Available: X-ray crystallographic files in CIF format for complexes $[Fe_6O_2(OH)_2(O_2CBu^t)_{10}(hep)_2]$ (**1**), $[Fe_6O_2(OH)_2(O_2CPh)_{10}(hep)_2]$ (**2**), $[Fe_6O_2(OH)(O_2CBu^t)_9(hep)_4]$ (**3**), and $[Fe_6O_2(OH)(O_2CPh)_9(hep)_4]\cdot 3MeCN$ (**4**·3 MeCN). This material is available free of charge via the Internet at http://pubs.acs.org.

IC049413H